The Late Neogene plate motion of North America as a consequence of the rotation of the Pacific plate: insights from modelling

MSc thesis by Willemse, M.F.M., Utrecht University

Supervisor: Dr. Iaffaldano, G. (University of Copenhagen)

April 22, 2020

Abstract

High-resolution plate motion reconstructions enable us to observe rapid plate motion changes on a geological time scale. The North American plate has changed its absolute motion between 8 and 5 million years ago (Iaffaldano and DeMets, 2016). The aim of this study is to explain this event through a reconstruction of torques associated with forces acting on the plate boundary. Two hypotheses are tested. The first hypothesis considers the motion change of the Pacific plate as the cause of the North American plate motion change. The clockwise rotation of the neighbouring Pacific plate occurred simultaneously with the motion change of North America. In the second hypothesis it is proposed that the motion change is a result of the plate boundary transformation of a diffuse to a strike slip margin in California due to the opening of the Gulf of California. In the Late Neogene the boundary in California migrated and a diffuse boundary developed to a strike slip fault. For both hypotheses the torque that the Pacific plate exerts on the North American plate is calculated. This is done for before and after the absolute motion change of North America. A numerical model of the Pacific-North America plate boundary is used. The torques are based on the strength of the lithosphere and the relative motion between the plates. The torque difference is then used to calculate the induced Euler vector change of North America. For the first hypothesis the modelled motion change of North America does not correspond with the observations from plate reconstructions. The results do not support the Pacific plate rotation as a cause of the North American motion change. The hypothesis of the tectonic evolution in California as a cause is a more plausible explanation. The direction and magnitude of the modelled Euler vector change of North America match the observations within the 68 percent confidence interval. Although some uncertainties remain, the applied method provides a good insight into the torques behind rapid plate motion changes.

1 Introduction

A lot of progress has been made in plate motion reconstructions which allows us to describe plate motions at a scale of 1 million years. Recent studies collected high-temporal-resolution finite rotations from magnetic anomalies along mid-ocean ridges (DeMets and Merkouriev, 2016; Croon et al., 2008). Iaffaldano and DeMets (2016) used data of seafloor spreading centres from several independent plate boundaries to constrain the North American plate motion in the Late Neogene. The authors combined the high-resolution relative motions and concluded that the solution for the North American plate motion was non-unique. Then, it was argued that the simplest scenario to explain the observed changes in relative motion was an absolute plate motion change of the North American plate. This change of motion occurred in a period between 8 and 5 Ma. The overall North American absolute velocity decreased. At the location of the San Andreas Fault the motion changed from 32 to 19 mm/year (Iaffaldano and DeMets, 2016). In Chapter 2 the applied method and findings of Iaffaldano and DeMets (2016) are further elaborated.

The goal of this study is to explain the North American absolute motion change in the Late Neogene. Two different hypotheses are tested. The first hypothesis involves the rotation of the neighbouring Pacific Plate around 6 Ma. This plate motion change was described by studies of hotspot tracks (Cox and Engebretson, 1985), magnetic anomaly data (Cande et al., 1995; DeMets and Merkouriev, 2016) and was linked to the reorganization of stress at several places along the plate margin, like the Gulf of California (Oskin and Stock, 2003b; Austermann et al., 2011). The Pacific plate rotated about 8 degrees clockwise with a rate of 47.8 mm/year relative to North America (DeMets and Merkouriev, 2016). The North American plate has a long and continuous shared boundary with the Pacific plate, mainly consisting of convergent and transform faults. Iaffaldano and DeMets (2016) speculated based on the timing of previously discussed events and the nature of the Pacific-North American plate boundary that the Pacific plate rotation could have been the cause of the Late Neogene North American plate motion change. Due to the rotation, the relative motion between the Pacific and

North American plate at the boundary changed in direction and magnitude. In this scenario, the Pacific plate motion change led to a redistribution of forces on the Pacific-North American plate contact which allowed the North American plate to change its motion. The hypothesis is in this study referred to as the Pacific hypothesis. The outcomes of this study did not confirm the hypothesis.

After it turned out that the results did not support the scenario of the Pacific plate rotation as the cause of the North American motion change, a second hypothesis was introduced. This hypothesis is related to a major reorganization of the Pacific-North American plate contact in California around the same time as the North American motion change. The Gulf of California began to open around 6 Ma (Oskin and Stock, 2003b). Within the few million years prior to this event, the Pacific-North America plate boundary migrated towards the East where it lies today. This led to a transformation from a diffuse into a fully developed strike slip boundary in California. As a result the plate boundary weakened substantially. This weakening affected the force that the Pacific Plate exerted on the boundary with North America. This could have caused the North American plate to change its motion. This scenario is in this study referred to as the California hypothesis. The results of this study support the hypothesis.

Figure 1: Map of the study region.The brown lines mark the tectonic plate boundaries. PA: Pacific plate, NA: North American plate, CO: Cocos plate, Ca: Caribbean plate, OK: Okhotsk plate and JDF: Juan de Fuca plate. Location of plate boundaries is taken from Bird (2003).

2 The Late Neogene Pacific-North American boundary and plate motion in the literature

2.1 Setting

An overview of the Pacific-North American plate boundary and adjacent tectonic plates is shown in Figure 1. The Pacific-North American plate boundary stretches for more than 11,000 kilometers. In the west the North American plate is bounded by the Okhotsk plate. To the South of North America lies the Cocos plate. The Pacific-North American plate contact is complex with alternating convergent and transform margins. In the North the oceanic Pacific plate subducts beneath the North American plate in the Aleutian trench. To the East the plate contact is mainly characterized by large right-lateral transform faults, including the Queen Charlotte and San Andreas Fault. In between lies the Cascadia subduction zone where the Juan de Fuca plate subducts below the North American plate. In the South (Gulf of California) the plate boundary continues into the East Pacific Rise.

For this study, it is important to know what the tectonic situation in terms of plate motions was at the Pacific-North American plate boundary in the Late Neogene. First, the evidence and timing of the North American plate motion change is discussed. Then, the Pacific plate rotation is reviewed, as in the Pacific hypothesis this event is proposed to be the cause of the motion change of North America. Finally, the tectonic developments around the opening of the Gulf of California are explained which play a central role in the California hypothesis.

2.2 Evidence for the North American absolute plate motion change

Iaffaldano and DeMets (2016) derived the absolute motion change of the North American plate based on relative motions derived from magnetic anomalies along several spreading ridges. High-resolution reconstructions from Eurasia-North America, Nubia-North America, Nubia-Antarctica, Somalia-Antarctica and Somalia-India from previous studies (DeMets et al., 2015a,b) were analysed and compared. Bayesian inference was implemented to measure the probability of each kinematic change (Iaffaldano et al., 2014). The authors found that it was likely that North-America changed its motion relative to Eurasia and Nubia by the same amount somewhere between 8 and 5 Ma. This motion change lasted about 0.1 Myr. Besides, in the same time-interval, it was found that it was probable that Antarctica changed its motion relative to both Nubia and Somalia with the same amount. These observations were combined to infer absolute motions. Any relative motion between two plates can be regarded as the result of the absolute motions

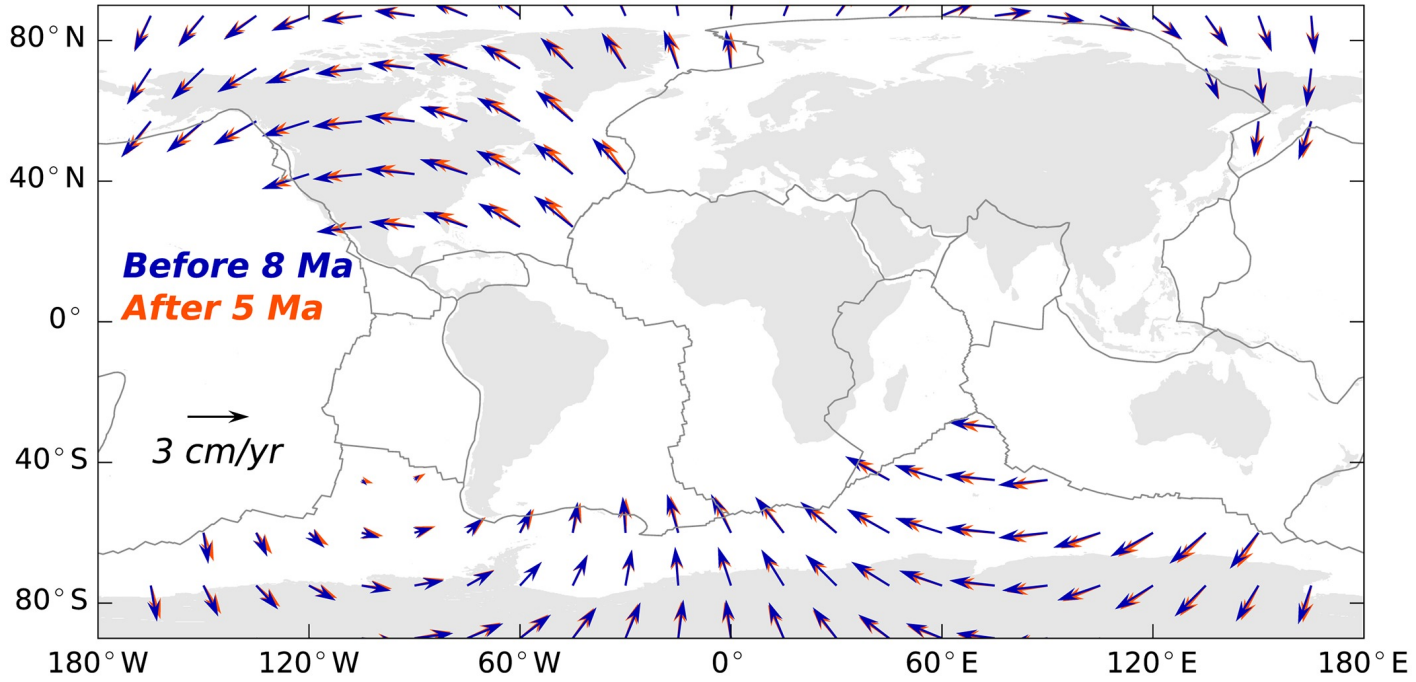

Figure 2: Absolute motions of the North American and Antarctic plate. Both the velocities before 8 Ma (blue arrows) and after 5 Ma (red arrows) are shown. Figure is from Iaffaldano and DeMets (2016).

of each individual plate. For example, the relative motion between plates A and B is equal to the difference between the absolute motions of plate A and B: $\Delta\omega_{A/B} = \Delta\omega_A - \Delta\omega_B$. Combining this with the aforementioned observations of relative plate motions, the authors prepared the following set of equations:

$$\Delta\omega_{NB} - \Delta\omega_{NA} = \Delta\omega_{EU} - \Delta\omega_{NA}$$
$$\Delta\omega_{NB} - \Delta\omega_{AN} = \Delta\omega_{SO} - \Delta\omega_{AN}$$
$$\Delta\omega_{SO} = \Delta\omega_{IN}$$

Where in this case $\Delta\omega$ represents the absolute motion change of a tectonic plate between 8 and 5 Ma. The captions NB, NA, EU, AN, SO, IN denote Nubia, North America, Eurasia, Antarctica, Somalia and India, respectively. The relative motion between Somalia and India was added as an additional constraint. The solution of this problem was non-unique with two different options. The first solution required that Eurasia, Nubia, Somalia and India all changed their absolute motion at the same time by the same amount. This was highly unlikely as these plates are influenced by different tectonic forces. The second solution was that only North America and Antarctica changed their absolute motion between 8 and 5 Ma. This solution was more probable as it was a simpler scenario which involved less plates changing their motion by exactly the same amount. Therefore the authors concluded that North America and Antarctica changed their absolute motions between 8 and 5 Ma. Because the North American absolute plate motion change was derived from magnetic anomaly data, rather than from an absolute reference frame, the Euler vectors are accurate with a low uncertainty. A visualisation of these plate motion changes is shown in Figure 2. Overall, the absolute plate velocity of North America decreased with around 5 mm/year. In the region of the San Andreas Fault the motion decreased from 32 to 19 mm/year. In the next paragraph the timing and magnitude of the motion change of the neighbouring Pacific plate are discussed.

2.3 Evidence for the Pacific plate rotation

2.3.1 Plate margin observations

Evidence for the Late Neogene rotation was derived from magnetic anomalies and a multibeam survey in the Pitman Fracture Zone, located on the Pacific-Antarctic Ridge (Cande et al., 1995). The orientation of the strike of the fracture zone showed an abrupt change in a clockwise direction. The interpreted change of strike between 6.04 and 5.11 Ma was 8 degrees. After the change of strike, the orientation of the Pitman Fracture Zone stabilized and remained unchanged. Other evidence comes from the Gulf of California. Various studies described a reorganization of stresses linked to the Pacific plate rotation. Before 6.3 Ma, slip along the Pacific-North American plate boundary was accommodated outside the Gulf of California (Fletcher et al., 2007). Sudden reorganization took place and displacement was localized within the Gulf of California (Oskin and Stock, 2003a,b). This was followed by the opening of Gulf of California (Umhoefer, 2011; Van Wijk et al., 2017). Finally, evidence for the Pacific plate rotation comes from the Lau Basin. This basin is located at the Australian-Pacific plate

contact, west of the Tonga trench. Bevis et al. (1995) concluded based on geodetic observations that around 6 Ma the Lau back-arc basin opened. Austermann et al. (2011) linked this event to the Pacific plate motion change. Based on the aforementioned studies, Austermann et al. (2011) concluded that the clockwise Pacific plate rotation was abrupt and occurred around 6 Ma.

2.3.2 Euler vector reconstructions

Different evidence for the Pacific plate motion change comes from plate reconstructions derived from magnetic anomaly data at ridges. High-resolution finite rotations of the Pacific-Antarctic relative motion do not describe any abrupt change around 6 Ma (Croon et al., 2008). DeMets and Merkouriev (2016) reconstructed the Pacific-North America relative motion through magnetic anomaly data from ridges which resulted into a 1 Myr resolution Euler vector reconstruction of the past 20 million years. Instead of an abrupt plate motion change, the reconstruction showed a gradual clockwise rotation of the Pacific plate. Since the last 8 Ma, the Pacific plate rotated 7 – 8 degrees relative to the North American plate. The rate of motion remained steady at an average of 47.8 mm/year. Furthermore, the authors argued that the observations of magnetic anomaly and multibeam data at the Pitman Fracture Zone (Cande et al., 1995) could be interpreted differently. Instead of just focusing on the orientation of the abyssal hills adjacent to the Pitman Fracture Zone before and after 5.9 Ma, a whole range of structures can be identified. According to DeMets and Merkouriev (2016), these abyssal hills show a gradual clockwise motion instead of an abrupt plate motion change.

The previously mentioned evidence described the Pacific plate motion in a reference frame relative to other plates. Independent constraints can be derived from plate reconstructions relative to hotspots in the mantle. Several hotspot seamount chains lie on the Pacific plate which were used in the past to reconstruct the Pacific absolute plate motion (Cox and Engebretson, 1985; Koppers et al., 1998; Wessel and Kroenke, 2008). Wessel and Kroenke (2008) studied and combined the tracks of 12 different seamount chains to construct finite rotations with a resolution of a few million years. The authors estimated that the clockwise rotation of the Pacific plate occurred around 6 Ma. Stotz et al. (2017) reconstructed the Pacific plate absolute motion since 15 Ma by combining several finite rotation data sets. This included the use of the absolute plate motion change of Antarctica between 8 and 5 Ma identified by Iaffaldano and DeMets (2016). Then, the authors combined the Antarctica plate motion change with the average absolute Antarctica motion since 10 Ma (Torsvik et al., 2010) to construct an Euler vector which described the absolute Antarctica motion from 5 Ma to the present. By adding the Euler vectors of the absolute Antarctica motion and the Pacific-Antarctica relative motion (DeMets and Merkouriev, 2016) the Pacific absolute motion was reconstructed. Stotz et al. (2017) concluded that most of the Pacific plate motion change occurred between 10-5 Ma.

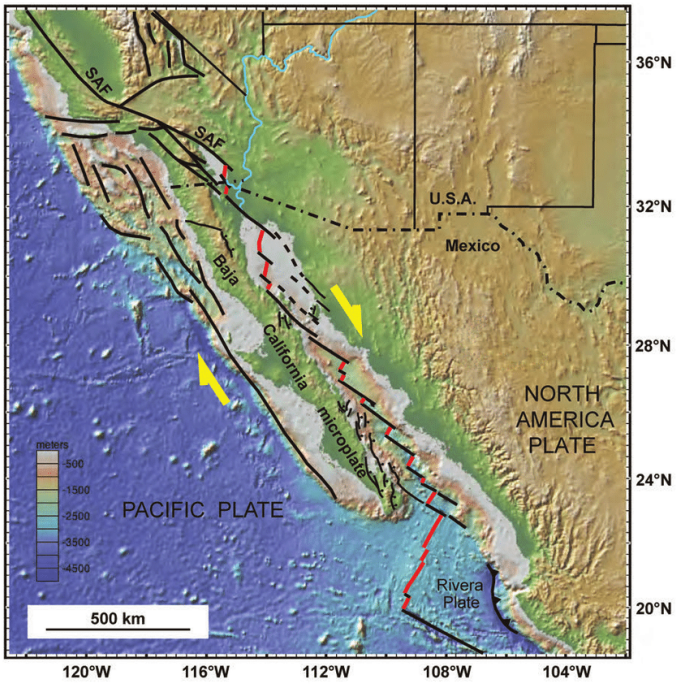

Figure 3: Present day tectonic map of the California region. Faults are shown in black lines, spreading centers in red. The yellow arrows mark the direction of the relative motion. SAF: San Andreas Fault. Figure adapted from Umhoefer (2011).

In the previous paragraphs different types of evidence for the Late Neogene Pacific plate rotation were discussed. The motion change occurred most likely around 6 Ma. It is debated whether the absolute motion change happened gradually or abrupt. The Pacific rotation affected the rate and direction of the relative motion along the whole plate boundary with North America.

2.4 Hypothesis 2: the Gulf of California

The region which experienced most tectonic evolution during the North American plate motion change was the Gulf of California and the surrounding area. This development plays a central role in the California hypothesis. A tectonic map of the region is shown in Figure 3. Extension in the Gulf of California developed gradually and the northern part eventually began to open around 6 Ma (Oskin and Stock, 2003b; Umhoefer, 2011). This event was preceded by a drastic reorganization of tectonic forces at the plate boundary. Prior to 12 Ma, the remaining part of the Farallon plate was subducting below the North American continental margin along Baja California. The plate contact was located to the West of the peninsula, rather than to the East where the Pacific-North American plate boundary

lies today. The oblique subduction was accompanied by the interaction of the Pacific-Farallon spreading ridge with the North American plate boundary. The subduction in that area ceased and around the same time spreading stopped. The exact order and timing of events regarding the Farallon plate in this region is debated (Michaud et al., 2006).

Over the course of a few million years, the boundary changed from an oblique subduction zone to a dextral strike-slip transform fault. Simultaneously, the boundary migrated from the west coast towards the East of Baja California (Stock and Hodges, 1989). In the North of the Gulf of California the boundary moved towards the present day location of the San Andreas Fault. This meant that in California the North American plate developed from a continuous continental lithosphere to an active strike slip boundary. The lithosphere in the Gulf of California ruptured and spreading followed (Umhoefer, 2011). Since the onset of the dextral strike-slip motion, it was estimated that Baja California migrated about 300 kilometer in a North-West direction along the boundary (Oskin et al., 2001). In California the motion was accommodated along the San Andreas Fault.

3 Method

3.1 Describing torques on plates

The motion change of a tectonic plate is the result of a change of the forces which affect the plate. Each of these forces exerts a torque, or moment upon the plate. The next paragraphs explain how to describe these torques quantitatively and how to estimate their magnitudes. For the explanation the approach of Iaffaldano and Bunge (2015) is followed.

3.1.1 Quantifying torques on plates

The net (or total) torque $\mathbf{M}_T$ acting on a plate can be divided into two different components. These are the torques caused by shallow-seated (tectonic) forces ($\mathbf{M}_N$) and the torques caused by basal-shear (asthenosphere) forces ($\mathbf{M}_b$).

$$\mathbf{M}_T = \mathbf{M}_N + \mathbf{M}_b \tag{1}$$

It can be demonstrated that at every moment in time a torque balance exists. A derivation of this is shown in Appendix B. Equation 1 reduces to:

$$\mathbf{M}_N + \mathbf{M}_b = 0 \tag{2}$$

This torque balance is essential; now the different torque components $\mathbf{M}_N$ and $\mathbf{M}_b$ can be defined and a physical expression for the total torque can be found. The torque related to basal-shear stresses can be described as follows:

$$\mathbf{M}_b = \int_A \mathbf{r} \times \boldsymbol{\sigma} \cdot dA = \int_A \mathbf{r} \times \mu \dot{\boldsymbol{\epsilon}} \cdot dA \tag{3}$$

Here $\mathbf{r}$ is the Earth's radius minus the local plate thickness. $\boldsymbol{\sigma}$ is the shear traction from the plate (with basal area A) gliding over the asthenosphere. Therefore this term represents the Couette flow in the mantle caused by the motion of the tectonic plate. Linear viscous flow is assumed. This makes that the shear traction is directly proportional to the strain rate $\dot{\boldsymbol{\epsilon}}$ through the viscosity μ. Equation 3 can be expressed in terms of the plate velocity:

$$\mathbf{M}_b = \int_A \mathbf{r} \times \mu_a \frac{\mathbf{v}_a - \mathbf{v}_p}{D} \cdot dA \tag{4}$$

Where $\mathbf{v}_p$ is the velocity of the plate at $\mathbf{r}$ relative to the mantle below the asthenosphere. $\mathbf{v}_a$ is the asthenosphere flow. D is the thickness of the asthenosphere. μ_a is the local radial average of the asthenospheric viscosity. The plate velocity $\mathbf{v}_p$ can be written in terms of angular velocity $\boldsymbol{\omega}$ which is also relative to the mantle below the asthenosphere. A cross product is applied here because the velocity $\mathbf{v}_p$ is a vector perpendicular to both $\mathbf{r}$ and $\boldsymbol{\omega}$.

$$\mathbf{v}_p = \boldsymbol{\omega} \times \mathbf{r} \tag{5}$$

This is used to get an expression for the angular velocity in Equation 4:

$$\mathbf{M}_b = \int_A \mathbf{r} \times \mu_a \frac{\mathbf{v}_a}{D} \cdot dA - \int_A \mathbf{r} \times \mu_a \frac{\boldsymbol{\omega} \times \mathbf{r}}{D} \cdot dA \tag{6}$$

Equation 6 can be substituted into Equation 2, and with rewriting the equation becomes:

$$\int_A \mathbf{r} \times \mu_a \frac{\boldsymbol{\omega} \times \mathbf{r}}{D} \cdot dA = \mathbf{M}_N + \int_A \mathbf{r} \times \mu_a \frac{\mathbf{v}_a}{D} \cdot dA \tag{7}$$

This is a useful expression as it relates plate motions on the left hand side to torques arising from tectonic forces and asthenospheric flow on the right hand side of the equation.

3.1.2 Torque difference due to a plate motion change

As was stated previously, at every moment in time the torques working on a tectonic plate are in balance. When the motion of a plate changes, a balance of torques can be constructed for both before (t_1) and after (t_2) the plate motion change.

$$\int_{A_1} \mathbf{r} \times \mu_a \frac{\boldsymbol{\omega}_1 \times \mathbf{r}}{D} \cdot dA_1 = \mathbf{M}_N(t_1) + \int_{A_1} \mathbf{r} \times \mu_a \frac{\mathbf{v}_a(t_1)}{D} \cdot dA_1$$

$$\int_{A_2} \mathbf{r} \times \mu_a \frac{\boldsymbol{\omega}_2 \times \mathbf{r}}{D} \cdot dA_2 = \mathbf{M}_N(t_2) + \int_{A_2} \mathbf{r} \times \mu_a \frac{\mathbf{v}_a(t_2)}{D} \cdot dA_2$$

These equations can be subtracted to describe the change of torques over time. While doing so, it must be assumed that the surface of the plate remains the same ($A_1 = A_2$). For rapid plate motion changes over a relatively short time interval this is a reasonable assumption. The torque change

can be expressed as follows:

$$\int_A \mathbf{r} \times \mu_a \frac{\Delta\boldsymbol{\omega}(t_1,t_2) \times \mathbf{r}}{D} \cdot dA = \Delta\mathbf{M}_N(t_1,t_2) + \int_A \mathbf{r} \times \mu_a \frac{\Delta\mathbf{v}_a(t_1,t_2)}{D} \cdot dA \quad (8)$$

Equation 8 shows that changes of the angular velocity of a tectonic plate are caused by either a change of torque due to tectonic forces, or by a change of torque due to the asthenospheric flow.

3.1.3 Application to the Pacific-North America plate boundary

The equations described in the previous paragraphs provide the framework to describe the torques at the Pacific-North America plate contact. For both the Pacific hypothesis and the California hypothesis the same mathematical approach is applied. The torque balance at two different moments is considered. These moments are before (t_1= 8 Ma) and after (t_2= 5 Ma) the absolute motion change of the North American plate. When Equation 8 is applied to this situation, a few terms can be simplified. With rapid plate motions, as is the case with North America, it is not expected that the flow in the asthenosphere changes significantly within the short time interval. This has to do with the scale of mantle convection. Numerical models of mantle circulations show that the timescale for large changes in mantle structure far exceeds the timescale of rapid plate motion changes (Bunge et al., 1998). Therefore it is assumed that for the case of North America $\Delta\mathbf{v}_a(t_1,t_2)$ is zero. Equation 8 reduces to:

$$\int_A \mathbf{r} \times \mu_a \frac{\Delta\boldsymbol{\omega}(t_1,t_2) \times \mathbf{r}}{D} \cdot dA = \Delta\mathbf{M}_N(t_1,t_2) \quad (9)$$

The next step is to get more insight into the term $\Delta\mathbf{M}_N(t_1,t_2)$ which describes the torque change due to tectonic forces. When the Pacific plate rotated, the magnitude of the torque exerted by the Pacific plate on North America changed. This is a result of the change of the resisting force of the Pacific plate on the boundary with North America. When the torques at the plate boundary before and after the North American motion change are compared, a tectonic torque difference remains which is a result of this resisting force change. In the hypotheses of this study it is assumed that $\Delta\mathbf{M}_N(t_1,t_2)$ is equal to the torque difference arising from the change in resisting force caused by the rotation of the Pacific plate. With this comes the assumption that all other torques arising from tectonic forces working on the plate boundary have not changed between 8 and 5 Ma.

Like any force, the resisting force the Pacific plate exerts on North America has both a magnitude and direction. The magnitude of this force is equal to the strength of the Pacific plate at the boundary, in this case denoted with $S(t,x)$. The strength of the boundary depends on the location along the plate contact and the moment in time. The direction of the resisting force is specified by the relative motion between the Pacific and North American plate. This direction can be represented by the unit vector $\hat{\mathbf{v}}(t,x)$ which is also dependent on time and the location along the plate boundary. The vector of the resisting force at one segment of the boundary is equal to the unit vector multiplied with the lithosphere strength and the length of the segment dx :

$$\mathbf{F}(t,x) = S(t,x) \cdot \hat{\mathbf{v}}(t,x) \cdot dx \quad (10)$$

The torque resulting from this force is the cross product with the radius $\mathbf{r}$. The total torque caused by the resisting force of the Pacific plate is equal to the sum of the individual torques related to each segment of the plate boundary. The total torque can be described as follows:

$$\mathbf{M}(t) = \int_L \mathbf{r} \times \mathbf{F}(t,x) \cdot dL \quad (11)$$

Where L is the total length of the plate boundary. Equation 11 can be applied to the plate boundary at both t_1 and t_2. Subtracting these torques leads to $\Delta\mathbf{M}(t_1,t_2)$, the torque difference due to the rotation of the Pacific plate over the time period 8 to 5 Ma:

$$\Delta\mathbf{M}(t_1,t_2) = \mathbf{M}(t_1) - \mathbf{M}(t_2) \quad (12)$$

The final step in order to test the hypothesis is to calculate the change of angular velocity of the North American plate induced by the torque change. Important to note in this process is that the torque change calculated with Equation 12 is said to be equal to $\Delta\mathbf{M}_N(t_1,t_2)$ of Equation 9. Again, this works because it is assumed that the torque difference is completely caused by the change in resisting force due to the Pacific rotation. Equation 9 can be written in matrix-notation:

$$\Delta\mathbf{M} = \mathbf{C}\,\Delta\boldsymbol{\omega} \quad (13)$$

Where the matrix $\mathbf{C}$ represents the double cross product with $\mathbf{r}$. The term also includes the average radial viscosity of the asthenosphere μ_a and the depth of the asthenospheric flow D. The complete matrix looks as follows:

$$\mathbf{C} = \frac{\mu_a}{D} \begin{pmatrix} \int_A (y^2+z^2)dA & -\int_A xy\,dA & -\int_A xz\,dA \\ -\int_A xy\,dA & \int_A (x^2+z^2)dA & -\int_A xy\,dA \\ -\int_A zx\,dA & -\int_A yz\,dA & \int_A (x^2+y^2)dA \end{pmatrix}$$

In this case it is assumed that beneath the plate D and μ_a are uniform. The matrix $\mathbf{C}$ can then be inverted. The inverse of this matrix exists because as is shown in Equation 9, it involves the integral over A, the surface of the plate. The final equation becomes:

$$\Delta\boldsymbol{\omega} = \mathbf{C}^{-1}\,\Delta\mathbf{M} \quad (14)$$

Where $\Delta\boldsymbol{\omega}$ is the angular velocity change of the North American plate due to the change of resisting force of the Pacific plate. The magnitude and direction of this vector can be compared with the results of Iaffaldano and DeMets (2016) to argue whether the motion change of North America is caused by the rotation of the Pacific plate. The next paragraph will go into further depth on how to calculate $S(t.x)$, the strength of the lithosphere.

3.2 The strength of the lithosphere

For this study the strength of the lithosphere is important as it defines the magnitude of the resisting force of the Pacific plate at the boundary (Equation 10). Therefore it has a significant impact on the magnitude and direction of the torque resulting from this force. The strength can be calculated from a strength profile of the lithosphere, of which an example is shown in Figure 4. The total strength of the lithosphere is equal to the integral of the profile. This is the value which has to be overcome to allow differential motion between two plates along a given margin. In this study a model of the strength profile of the Pacific plate at the boundary with North America is built. The model can be distinguished into two different sections, based on the dominant rock deformation mechanism. The upper part of the profile contains brittle deformation, while the lower part of the profile is characterised by ductile deformation. The intersection between both lines marks the transition between the dominant deformation mechanism. The dotted line in Figure 4 shows how the value of the strength integral increases with depth. Most of the strength of the lithosphere lies in the region with brittle deformation. The ductile part of the profile is substantially weaker.

The Pacific plate at the boundary with North America exists of both oceanic and continental lithosphere. The type of lithosphere affects the shape and the integral of the strength profile. Besides, the profile is dependent on age which means it has different input values for different moments in the past. For the torque calculation the strength of the Pacific plate is required for both before (8 Ma) and after the North American plate motion change (5 Ma). In the following paragraphs the different factors influencing the lithosphere strength in the model are discussed. The complete list of input parameters and their values can be found in Table 2.

3.2.1 Temperature and pressure gradients

The temperature and pressure in the lithosphere control the type of rock deformation with depth. The temperature gradient in the model depends on the heat flow and thermal conductivity. For oceanic lithosphere, the heat flow in the model is derived from the cooling half-space model (Stein and Stein, 1992). Therefore the heat flow of the oceanic lithosphere of the Pacific plate is based on the age of the seafloor. Reconstructed age grids are used for 8 and 5 Ma

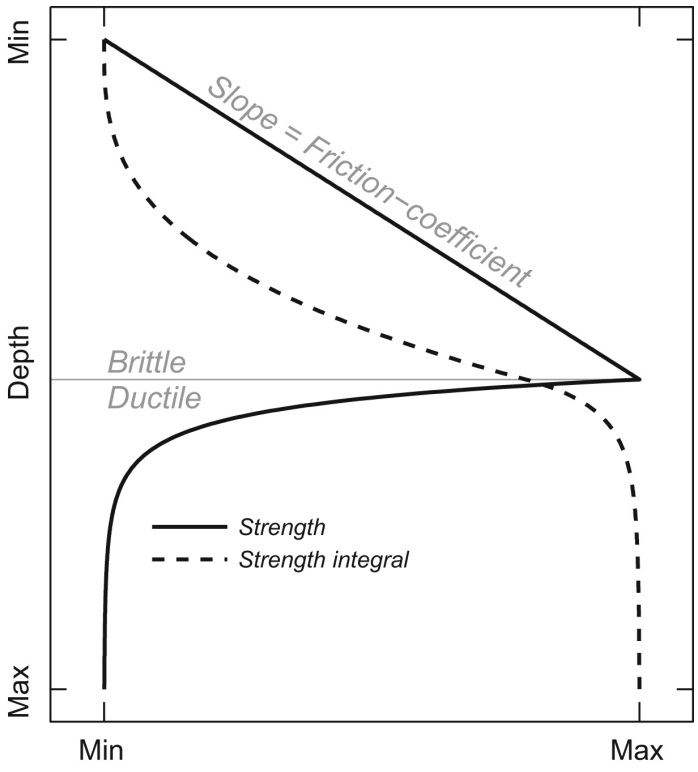

Figure 4: A typical strength envelop of rocks in the lithosphere. The dashed line shows the total integral as a function with depth. Figure from Iaffaldano (2012).

(Müller et al., 2008). For continental lithosphere, the heat flow is taken from a global heat flow database (Davies, 2013). The pressure gradient depends on rock density and increases with depth. The rock density is taken to be constant for each rock type.

3.2.2 Brittle deformation

In the upper part of the lithosphere rock deformation is controlled by frictional sliding (Kohlstedt et al., 1995) and the maximum differential stress in this region is referred to as the frictional strength. The frictional strength can be determined through the Mohr-Coulomb theory:

$$\sigma_s = S_0 + \mu\sigma_n \tag{15}$$

This linear relationship shows that three parameters contribute directly to the frictional strength: normal stress σ_n, cohesive strength S_0 and the coefficient of friction μ. The normal stress is equal to the component of pressure orthogonal to the fault surface of the plate boundary. In the model, the dip angle of this surface depends on the plate boundary type. The coefficient of friction has a large impact on the value of the frictional strength, but has shown to be difficult to constrain for large scale plate boundaries. The choice for the friction coefficient in the model is explained in the following paragraph.

Model	μ_{min}	μ_{max}	saturation thickness (km)
1	0.02	0.05	0.5
2	0.01	0.06	1
3	0.02	0.07	1

Table 1: Values for the friction models used in this study.

Often Byerlee's law is used to estimate the coefficient of friction for rocks at a certain pressure. This is a specific relation between maximum stress and the coefficient of friction based on numerous laboratory experiments and has shown to work well for a whole range of rock types (Byerlee, 1978). The typical value used for the coefficient of friction is 0.85 at low confining pressure ($<$ 200 MPa) and 0.6 at higher confining pressure ($>$ 200 MPa). However, these values were determined by measuring the strength of rock samples on a small scale in a laboratory and it is questionable whether these values reflect well on the actual strength of large-scale plate boundaries. Suppe (2007) studied the mechanics of critical taper wedges at accretionary wedges of converging plate boundaries. A relationship was found between the shape of the wedge and the wedge strength. From this the frictional properties of the margin were estimated. The coefficient of friction of the basal detachment lay between 0.04 and 0.1, which was considerably less than what was found in laboratory studies. Iaffaldano (2012) described the driving forces of the convergence between the Philippine plate and Eurasia in order to constrain the friction coefficient at the plate boundary. The study established a relationship between the sediment thickness on the ocean floor and the coefficient of friction of the plate boundary. This relationship stated that the friction coefficient decreased linearly with an increase of sediment thickness. The coefficient of friction was the highest when there was not any sediment present at the margin. The decrease continued to the point that a threshold thickness was reached for the sediments, referred to as the saturation thickness. From there the coefficient of friction stayed at a minimum value. Iaffaldano (2012) tested a range of values and three models gave results which correspond with the observed convergence rate. These models are shown in Figure 5 and their parameters are described in Table 1. Iaffaldano (2012) concluded that the value of the friction coefficient at large plate boundaries lay between 0.01 and 0.07. The magnitude of these values corresponds roughly to what Suppe (2007) proposed. The friction models are applied to the model of the strength profile for the brittle part of the oceanic lithosphere. For the continental margin a constant value is used, within the range of the values proposed by the previously discussed studies (Iaffaldano, 2012; Suppe, 2007).

3.2.3 Ductile deformation

With increasing pressure and temperature with depth, the dominating rock deformation mechanism changes to ductile deformation. The maximum differential stress σ_d in this region is called the plastic strength. In the lithosphere strength model the following law is used to describe the ductile deformation (Kohlstedt et al., 1995):

$$\sigma_d = \left(\frac{\dot{\epsilon}}{A} e^{\left(\frac{Q+PV_d}{RT}\right)} \right)^{\frac{1}{n}} \tag{16}$$

The parameters n, A, Q and V_d describe the ductile behaviour of a certain rock type and can be derived from laboratory experiments (e.g. Gleason and Tullis, 1995; Chopra et al., 1981). The explanation and input values of these parameters can be found in Appendix A. Each rock type has specific properties which affect the ductile deformation curve in the strength profile. For many rock types a number of laboratory experiment measurements is available from the literature (e.g. Burov, 2011). To account for the variety of measurement outcomes of these studies in the model, the strength profile is calculated for a range of different values. The average of the surface integral of these strength profiles is taken as the representative strength of the lithosphere. Besides, also the strain rate $\dot{\epsilon}$ influences the plastic strength. The strain rate in the context of plate boundaries can be regarded as the deformation rate at the plate contact. This local rate at the plate boundary is derived from the relative motion between the Pacific and North American plate. The strain rate is then achieved by dividing the rate of motion by the width of the plate boundary. The width of a plate boundary is generally in the order of a hundred kilometers and is taken as a constant along the margin.

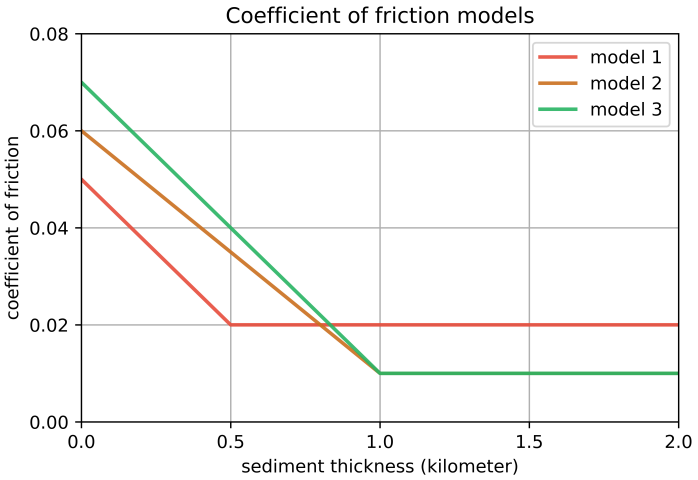

Figure 5: Models proposed by Iaffaldano (2012) for the coefficient of friction of large-scale plate boundaries as a function of sediment thickness.

3.2.4 Uncertainty of strength profile in the past

The model calculates the strength profile of the lithosphere in the past, rather than in the present, which brings some additional uncertainties. The exact thickness of sediment

which is used as an input for the coefficient of friction is unknown in the past. Therefore the model uses the present day sediment thickness based on the location of the plate boundary. This is a justifiable assumption as the location of the Pacific-North America plate boundary has not changed much since 8 Ma. Also the heat flow of the continental lithosphere in the past is difficult to constrain. The values of the heat flow are taken from a global present-day database (Davies, 2013). The heat flow data is based on a large set of point measurements. The values measured around the Gulf of California, however, are extremely high for continental lithosphere. Taken into account that these values are based on point measurements and today spreading is occurring in parts of the region, it is decided to limit the heat flow in the model to 75mW m^{-2}. This is in the order of what is expected for continental lithosphere (Pollack et al., 1993) and therefore a more representative approximation of the heat flow around 8 and 5 Ma.

Finally, examples of strength profiles along the Pacific-North American plate boundary generated by the model are shown in Figure 6.

3.3 Model input

3.3.1 Euler vectors

The Euler vectors of the Pacific-North American relative motion play an essential role in determining the torque change between both plates from 8 to 5 Ma. The direction of the resisting force at the plate contact corresponds with the direction of the relative motion. The torques are then derived from the cross product of this force with the position vector. Furthermore, from the same Euler vectors the strain rate is derived which is used in the lithosphere strength profile. In this study the relative motion between the two plates is reconstructed through their individual absolute plate motions. For the Pacific plate, the finite rotations of the WK08-G model of Wessel and Kroenke (2008) are used. For the North American plate, the finite rotations of Doubrovine et al. (2012) are used. This data was derived from a global moving hotspot reference frame and has a coarser resolution of a 10 million year timescale. From the finite rotations the stage poles are reconstructed for the plates at both 8 and 5 Ma. Once the stage poles for both plates are known these are used to calculate the relative motion between the two plates which is expressed as an Euler vector. To account for the uncertainty of the Euler vectors, an ensemble of one million samples is generated for each finite rotation. The generation of these samples is based on the covariance of the finite rotation. For all of these samples the stage poles of the relative motion are calculated. The input for the model is a set of one million samples of the Euler vector describing the relative motion between the Pacific and the North American plate.

The choice for absolute motions of the individual plates, rather than available relative motion data (DeMets and Merkouriev, 2016) can be motivated through the torque equations and the hypotheses. To describe the North American absolute motion change, Iaffaldano and DeMets (2016) partly used the same data as DeMets and Merkouriev (2016) did. Therefore, if the Pacific-North American relative motion data was used to determine the direction of the resisting force along the plate boundary in this study (e.g. Equation 10), it would already be imposed in the model that the North American motion change occurred. Instead, by using the absolute plate motions the output of the model is independent of the North American plate motion change. The data of Doubrovine et al. (2012) does not resolve the motion change and therefore the calculated torque difference is the result of the Pacific plate rotation alone.

3.3.2 Asthenosphere viscosity and thickness

The calculated change in torque in the model is converted to a change in angular velocity through the inverse of the matrix $\mathbf{C}$ (Equation 14). This matrix involves rheological parameters of the mantle such as the viscosity of the asthenosphere. Based on postglacial rebound studies and studies of the geoid it was concluded that a contrast of viscosities must exist between the asthenosphere and the mantle below. In terms of rheology, the asthenosphere is regarded as a 'low viscosity zone' (LVZ) (e.g. Cathles, 1975; Hager and Richards, 1989). In attempts to constrain these values it was found that there was a trade-off between the thickness of the LVZ and its viscosity (Cathles, 1975). The exact values for these parameters however remained to be a topic of debate as it is notoriously difficult to get high resolution constraints on the viscosity structure of the upper mantle (Mitrovica, 1996; Paulson and Richards, 2009; Peltier and Jiang, 1996). In the model of this study, the following relationship (Paulson and Richards, 2009) between the viscosity contrast with the LVZ and the mantle is used to constrain the thickness of the asthenosphere:

$$D = 10^{2.67} \left(\frac{\mu_a}{\mu_{um}} \right)^{0.337} \tag{17}$$

Where D and μ_a are the asthenosphere thickness and viscosity. μ_{um} is the viscosity of the upper mantle below the the LVZ. The model is run for different viscosity contrasts. The use of these contrasts result in four different viscosity models which are shown in Table 3. The viscosity values are in the order of a magnitude comparable with the outcomes of most postglacial rebound and geoid studies (Paulson and Richards, 2009; Richards and Lenardic, 2018).

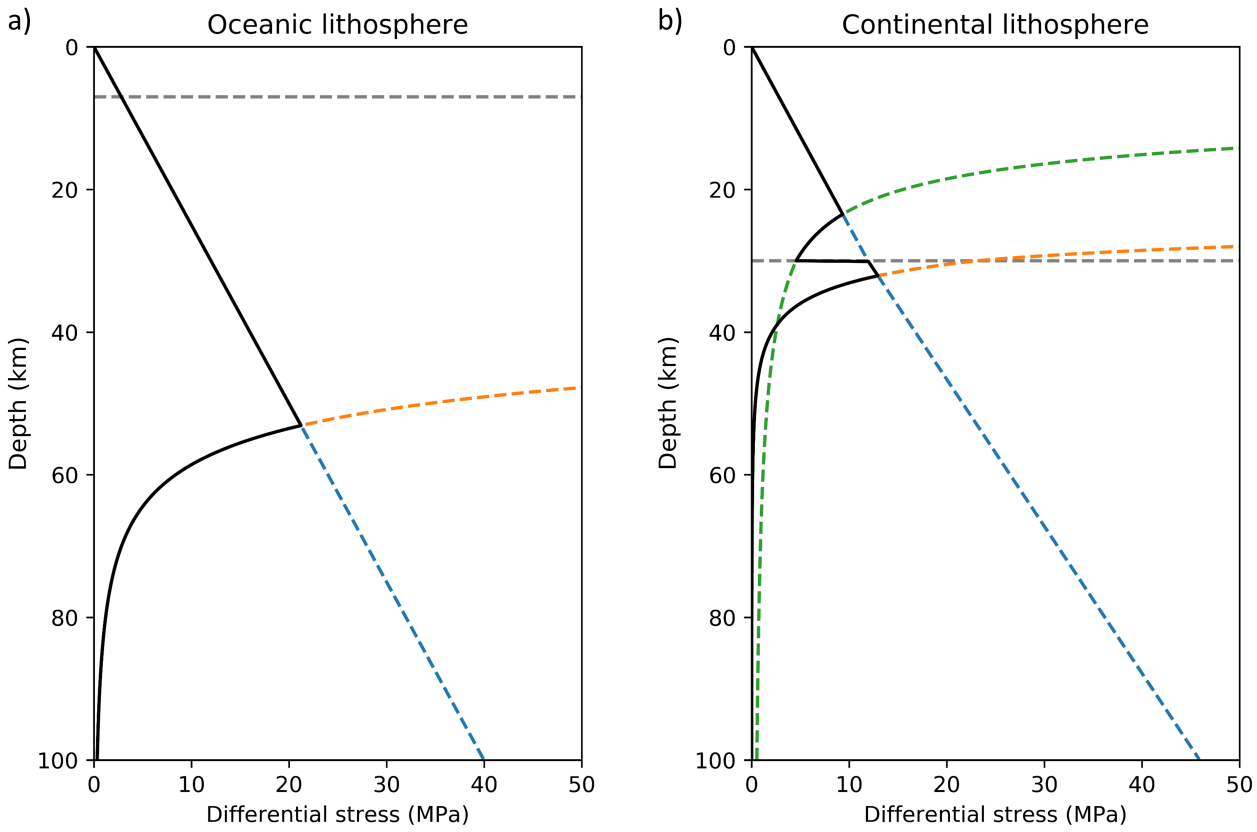

Figure 6: Examples of strength profiles of the lithosphere at the Pacific-North America plate boundary against depth. The strength profile is shown in black. The grey dashed line represents the depth of the Moho. The blue dashed line is the frictional strength and the orange and green lines represent the plastic strength. a) An oceanic lithosphere strength profile. b) A continental lithosphere strength profile.

General parameters			
Parameter	**Description**	**Value**	**Source**
n,A,Q,V_d	Ductile deformation parameters	-	See Appendix A
R	Gas constant	8,314 $J \cdot K^{-1} \cdot mol^{-1}$	
k	Thermal conductivity	crust: 2.75 lithospheric mantle: 3.5	McKenzie et al. (2005)
T_a	Asthenosphere temperature	1300 °C	
k	Thermal diffusivity	10^{-6} m$^2 \cdot s^{-1}$	Robertson (1988)
L	Lithosphere thickness	100 km	
W	Width of plate boundary	150 km	
ρ_m	Density mantle (Olivine)	3300 kg/m^3	

Oceanic Lithosphere			
Parameter	**Description**	**Value**	**Source**
Q	Heat flow	0-500 mW $\cdot$ m^2	Müller et al. (2008) (Seafloor age)
μ	Coefficient of friction	0.01-0.07	Iaffaldano (2012) Whittaker et al. (2013)(Sediment thickness)
z_m	Moho depth	7 km	White et al. (1992)
ρ_c	Density crust (Gabbro)	3300 kg/m^3	

Continental Lithosphere			
Parameter	**Description**	**Value**	**Source**
Q	Heat flow	0-75 mW $\cdot$ m^2	Davies (2013)
μ	Coefficient of friction	0.03	Suppe (2007); Iaffaldano (2012)
z_m	Moho depth	30 km	Christensen and Mooney (1995)
ρ_c	Density crust (Quartzite)	2700 kg/m^3	

Table 2: Input parameters for the model of the strength profile of the lithosphere.

Model number	μ_a (Pa s)	μ_{um} (Pa s)	D (km)
1	10^{20}	$5 \cdot 10^{21}$	187.8
2	10^{20}	$1.5 \cdot 10^{21}$	148.7
3	$5 \cdot 10^{19}$	$1.5 \cdot 10^{21}$	99.1
4	$5 \cdot 10^{19}$	$5 \cdot 10^{21}$	125.2

Table 3: Overview of the different viscosity models. μ_a: viscosity of the asthenosphere. μ_{um}: viscosity of the mantle below the asthenosphere. The asthenosphere thickness D is calculated with Equation 17.

In the following sections first the results for the Pacific hypothesis are presented and analysed. The model used to test this hypothesis is referred to as the Pacific model. Then the model (referred to as the California model) used for the California hypothesis is further elaborated and the results are discussed.

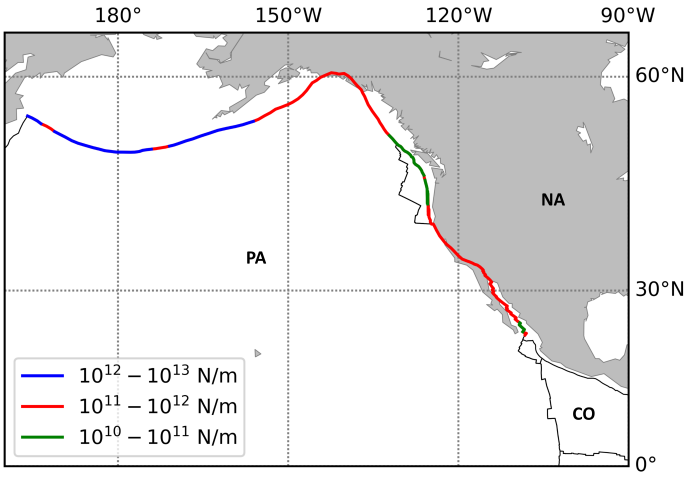

Figure 7: The strength of the lithosphere along the Pacific-North America plate boundary at 5 Ma. PA: Pacific plate, NA: North American plate, CO: Cocos plate.

4 Results Pacific hypothesis

4.1 Plate boundary strength and torques

The strength of the lithosphere varies along the Pacific-North American plate boundary. Figure 7 shows the calculated values of the strength integral along the plate boundary at 5 Ma. The units are in Newton/meter as this equals the differential stress (Pascal) times the depth of the profile. Strength differences of up to 2 orders of magnitude can be observed along the plate contact. The lithosphere is particularly weak near the Juan de Fuca plate and in the Gulf of California. The strength of the plate boundary and the direction of the relative motion determine the torque which the Pacific plate exerts on the North American plate. The torques are represented with a pole and a magnitude. The pole distribution and the magnitude of the torques are shown in Figure 8. The poles of the torques calculated at 8 Ma show a larger spreading than the the torques at 5 Ma. The poles of 5 Ma lie completely within the 8 Ma pole distribution. The magnitude of the torque at 5 Ma is larger than at 8 Ma. Both torques are in the order of 10^{25} Newton meter. The difference between both torques is used to calculate the Euler vector change.

4.2 Euler vector change

The distribution and magnitude of the Euler vectors which describe the motion change of North America are shown in Figure 9. The outcome of the model is shown together with samples of the Euler vector results of Iaffaldano and DeMets (2016). The distributions of the model outcome and the study results are far apart and the poles lie on different hemispheres. The peaks in the angular velocity histogram correspond well. The model has been tested for different input values for the viscosity and coefficient of friction. The applied friction models are listed in Table 1 and the viscosity models in Table 3. The coefficient of friction affects the strength of the plate boundary and therefore the calculated torque. This has an influence on the angular velocity of the motion change. The location of the Euler poles remain almost unchanged. The Euler pole distribution as a function of friction and viscosity can be found in Appendix C. The effect of the different friction models on the angular velocity is shown in Figure 10. What can be observed is that a different model shifts the peak of the angular velocity plot. The angular velocity is the highest when friction model 3 is applied. This model has the highest maximum coefficient of friction, which leads to a relatively large frictional strength in the profile. Friction model 1 contains the lowest maximum friction coefficient which leads to a lower angular velocity overall.

Figure 11 shows the angular velocity as a function of different viscosity models. Like with the friction models, the angular velocity peak is shifted. The effect on the longitude and latitude of the Euler poles is negligible (Appendix C). Viscosity model 2 has the smallest contrast between the viscosity values of the asthenosphere and the mantle. Viscosity model 4 has the largest contrast in values. However, the models which produce the smallest and largest angular velocity are viscosity models 1 and 3. Viscosity model 1 has the largest thickness of the asthenosphere and gives the lowest angular velocity. The angular velocity is the highest when viscosity model 3 is applied, which contains the smallest thickness of the asthenosphere.

5 Analysis of Results Pacific hypothesis

The strength of the lithosphere changes as the value of parameters change along the margin. In the North the subducting lithosphere is older which results in a lower

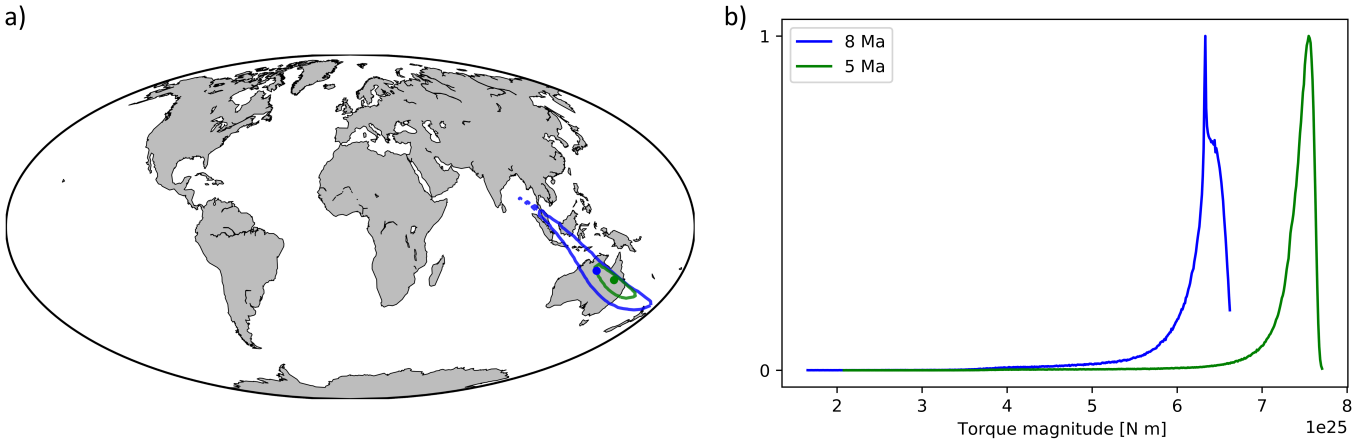

Figure 8: The distribution of calculated torques at 8 Ma (Blue) and 5 Ma (Green). a) The contours show the 68 percent confidence interval. The dots show the average values. b) The magnitude of the calculated torques. In this case friction model 2 is used.

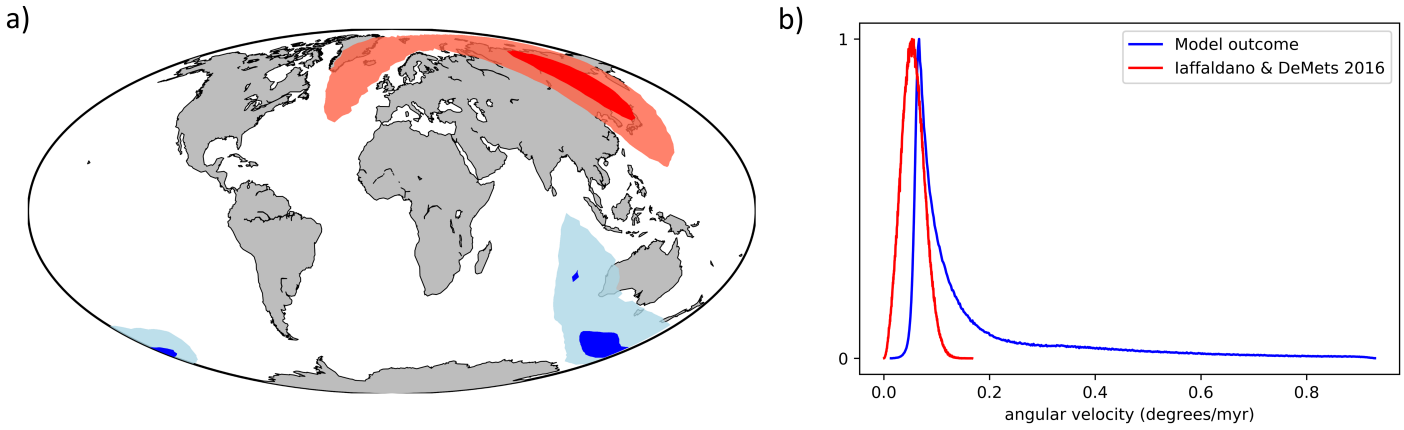

Figure 9: The Euler vectors of the North American absolute motion change. a) The results calculated by the Pacific model are shown for the 68 percent (light blue) and the 20 percent confidence region (dark blue). The results of Iaffaldano and DeMets (2016) are shown in red. b) Histogram of the angular velocity.

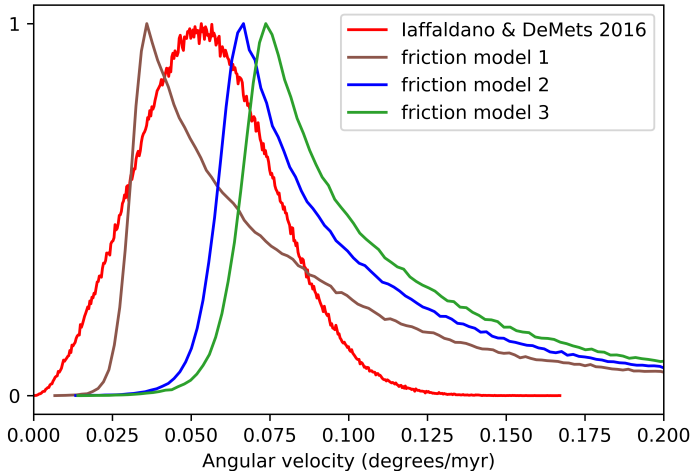

Figure 10: The angular velocity results of the Pacific model for different friction models. The distribution of the angular velocity of Iaffaldano and DeMets (2016) is shown in red.

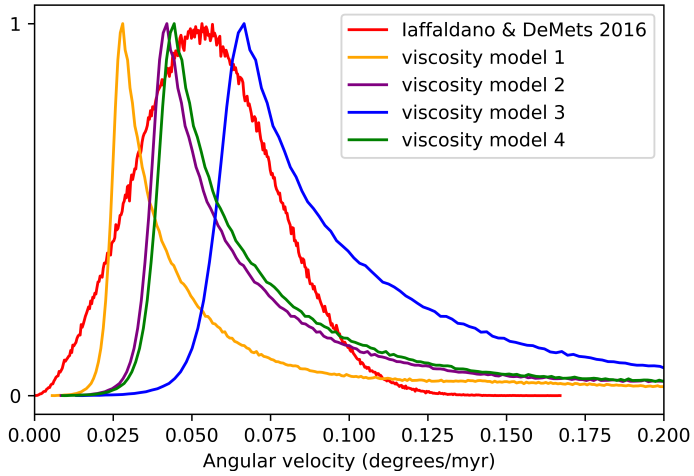

Figure 11: The angular velocity results of the Pacific model for different viscosity models. The distribution of the angular velocity of Iaffaldano and DeMets (2016) is shown in red.

heat flow. Therefore the lithosphere is relatively strong in that region. Along the Juan de Fuca plate and in the Gulf of California the lithosphere is young which explains the lower strength values in those regions. The magnitude of the calculated torques is in the order of magnitude what is expected for tectonic torques. The results of the Euler vector change of the North American plate due to the rotation of the Pacific plate have been presented. The locations of the Euler poles generated by the model do not fall in the 68 percent confidence interval of the Euler poles calculated by Iaffaldano and DeMets (2016) (Figure 9). If the Pacific plate rotation has caused the motion change of North America, it is expected that the locations of the Euler poles would correspond. However, the poles generated by the model are far off which means that the direction of the motion change induced by the Pacific plate is different.

The coefficient of friction and viscosity both influence the angular velocity in a similar way. The peak of the angular velocity is shifted towards the right or left side of the values of the Euler pole sampling of Iaffaldano and DeMets (2016). The friction coefficient affects the torque directly. Therefore the impact of the friction coefficient on the induced motion change emphasizes the importance of a good approximation of the torque. A larger friction coefficient leads to a larger angular velocity due to the larger strength of the lithosphere. The use of different viscosity models also results in a different angular velocity. The asthenosphere thickness is calculated based on the viscosity contrast of the models. This combination of factors plays a role in the conversion of the torque difference to the Euler vector change. The impact of the viscosity on the model is discussed in further depth in the general discussion (Chapter 9). The location of the Euler poles remains virtually unchanged. Therefore the poles from the model stay equally far off from the observed Euler poles. It can be concluded that the rotation of the Pacific plate did not cause the absolute motion change of North America in the Late Neogene. In the next paragraphs the setup and results of the second hypothesis are discussed.

6 Testing the California hypothesis

This part of the study focuses on the second hypothesis, whether the tectonic changes accompanied with the opening of the Gulf of California caused the North American plate motion change in the Late Neogene. The model which is used to test this hypothesis is referred to as the California model. The same mathematical approach is applied as with the Pacific model. Again the torque of the resisting force of the Pacific plate is calculated at both before (8 Ma) and after (5 Ma) the motion change of North America. The focus lies on the part of the plate boundary affected by the opening of the Gulf of California. The segment of the plate boundary used in the California model is shown in Figure 12. This margin migrated and transformed when Baja California migrated northwards. Therefore it experienced most tectonic evolution during the absolute motion change of North America between 8 and 5 Ma.

At 8 Ma it is assumed that the plate boundary in California is not fully formed yet. First it was located along the west coast, where there had been subduction. Then, the boundary migrated inland to the location where it is today. At 8 Ma the region was deforming but a complete lithosphere boundary was not yet developed. This situation is simulated in the model with a large coefficient of friction which creates a large resistance against brittle deformation. This means that more stress is required to allow relative motion between the plates and therefore this mimics the

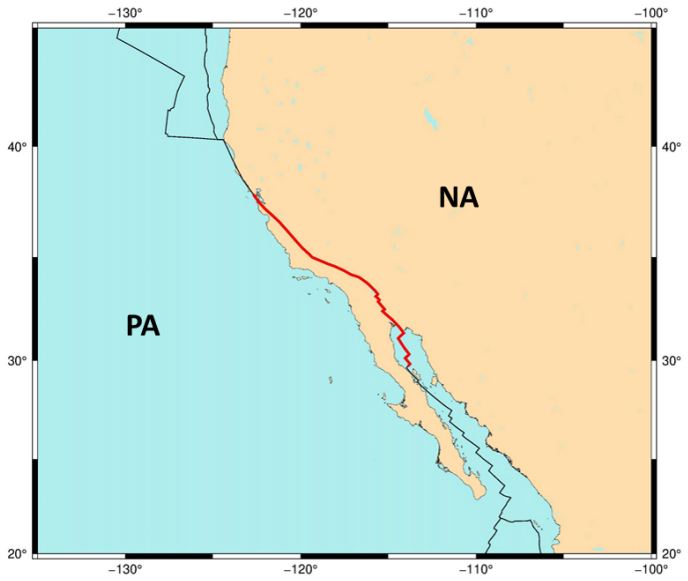

Figure 12: The present day Pacific-North America plate boundary around Baja California. The plate boundary is marked in black. The plate boundary segment used in the California model is shown in red. PA: Pacific plate, NA: North American plate.

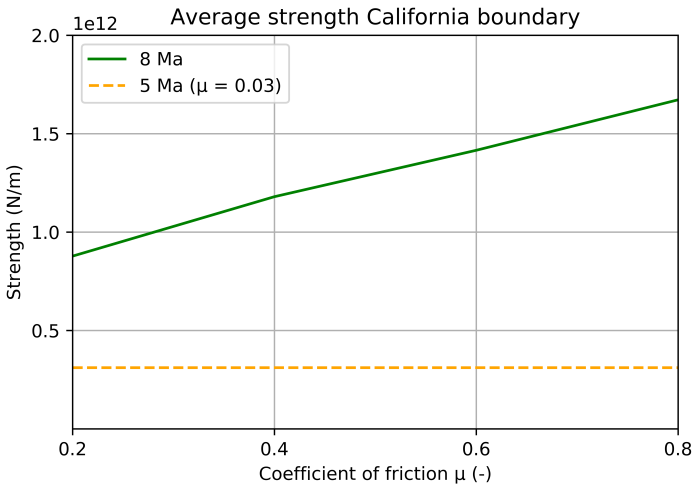

Figure 13: The average strength of the Pacific-North America plate boundary in California at 8 Ma as a function of friction coefficient is shown in green. For comparison, the orange dashed line shows the strength of the plate boundary at 5 Ma with a fixed friction coefficient of 0.03.

presence of the diffuse boundary. In the simulations the values 0.2, 0.4, 0.6 and 0.8 are used. These values are higher than what is thought to be reasonable for fully developed plate boundaries (Suppe, 2007; Iaffaldano, 2012) and are more in the range of the results of laboratory deformation experiments (Byerlee, 1978). At 5 Ma the continental margin has become a strike slip fault. For the coefficient of friction of continental lithosphere the same procedure is applied as with the Pacific model, a constant value is taken (Table 2). The torque difference predominantly arises from the large friction coefficient which is used to simulate the development of the margin between 8 and 5 Ma.

7 Results California hypothesis

7.1 Plate boundary strength and torques

The strength of the plate boundary is mainly controlled by the different friction coefficient values applied to the model at 8 Ma. The strength of the lithosphere as a function of the friction coefficient is shown in Figure 13. For 8 Ma, an increase of friction coefficient causes an almost linear increase of the average strength integral value along the California plate boundary section. Also the (fixed) strength of the plate boundary at 5 Ma is plotted. At 5 Ma a constant friction coefficient of 0.03 is used. The strength of the boundary at 8 Ma is for any of the tested friction coefficient values higher than the strength at 5 Ma. The torques calculated by the California model are shown in Figure 14. The direction is represented by the pole and the histogram shows the magnitude of the torques at 8 and 5 Ma. The uncertainty of poles at both times is relatively small. The torque magnitude histograms show very little individual spreading. The magnitude of the torques is in the order of 10^{24} to 10^{25} Newton meter. The torque at 8 Ma is significantly larger than the torque calculated at 5 Ma.

7.2 Euler vector change

Based on the torque difference the Euler vector change of North America is calculated. The Euler poles and angular velocity which describe this motion are shown in Figure 15. Besides the model outcomes also the sampled Euler poles of Iaffaldano and DeMets (2016) are plotted. The region of the 68 percent confidence interval of the model outcome overlaps with the sampled poles from the literature. The 20 percent confidence regions however, are far apart. The angular velocities correspond well. The California model has been tested for a range of friction and viscosity models. The value of the friction coefficient of the boundary at 8 Ma has been varied. The effect of of these values on the angular velocity is shown in Figure 16. Again, a different friction coefficient affects the strength of the lithosphere. As a result, a larger friction coefficient leads to a larger angular velocity. The Euler pole location is barely influenced by different friction coefficients. The effect of the friction coefficient on the Euler pole location can be found in Appendix C.

The same viscosity models have been applied to the California model as with the Pacific model. The models are listed in Table 3. The results for different viscosity models are shown in Figure 17. The viscosity input has a large influence on the peak of the angular velocity histogram.

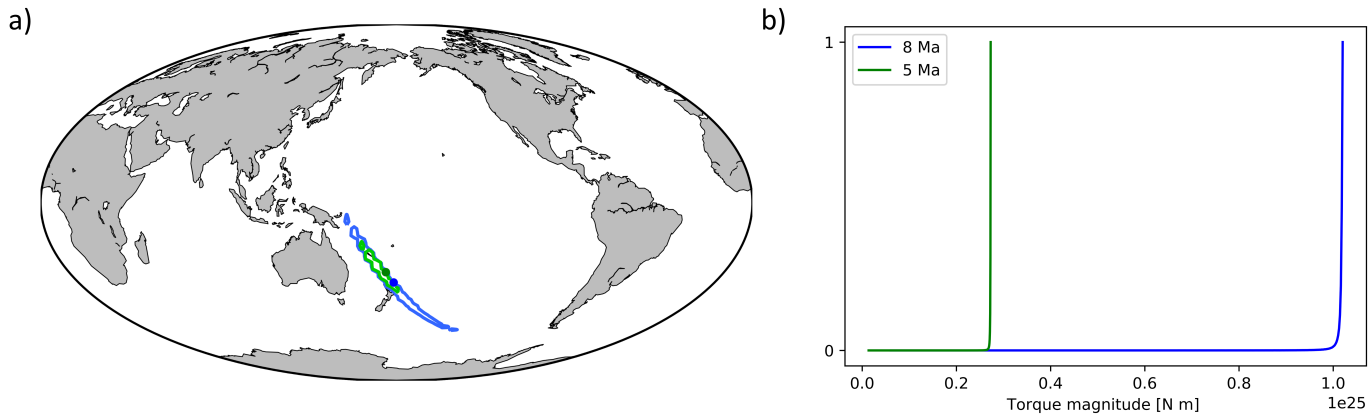

Figure 14: The distribution of calculated torques at 8 Ma (Blue) and 5 Ma (Green). a) The contours show the 68 percent confidence interval. The dots show the average values. b) The magnitude of the calculated torques.

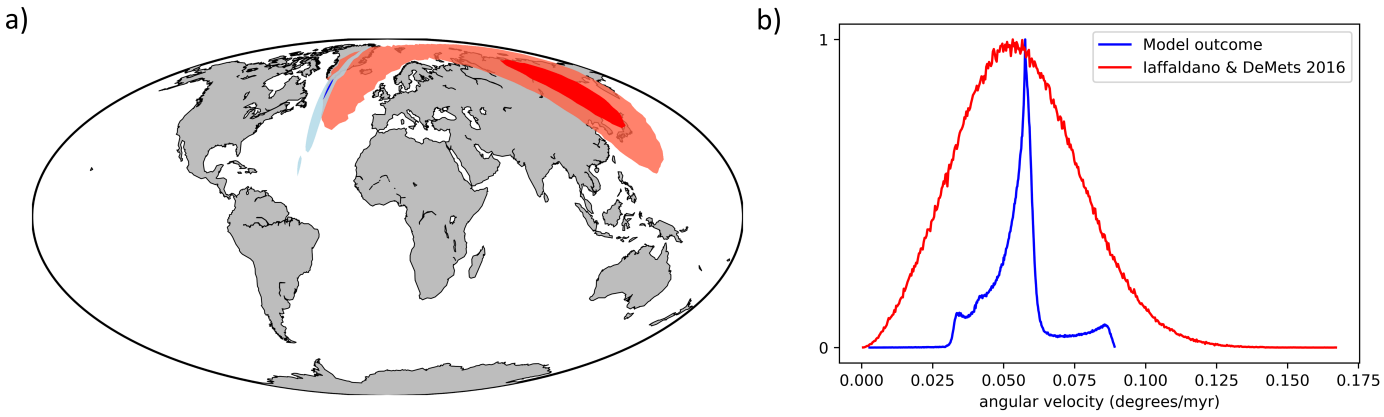

Figure 15: The Euler vectors of the North American absolute motion change. a) The results calculated by the California model are shown for the 68 percent (light blue) and the 20 percent confidence region (dark blue). The results of Iaffaldano and DeMets (2016) are shown in red. b) Histogram of the angular velocity.

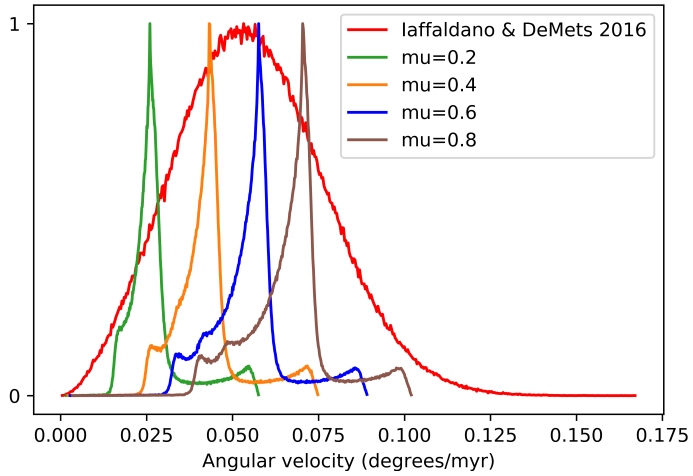

Figure 16: The angular velocity results of the California model for different models of the coefficient of friction. The distribution of the angular velocity of Iaffaldano and DeMets (2016) is shown in red.

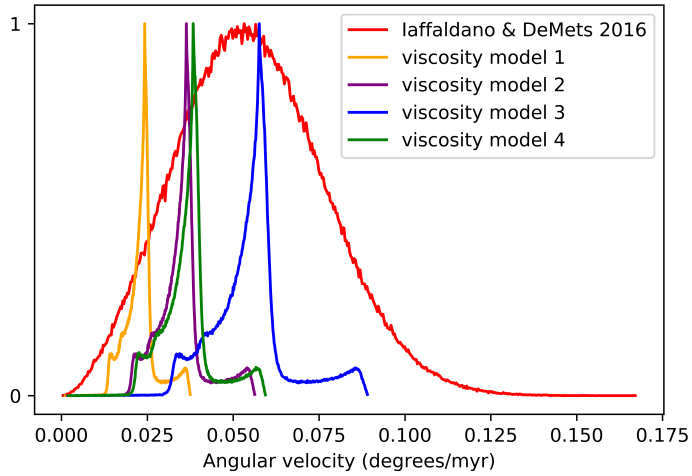

Figure 17: The angular velocity results of the California model for different viscosity models. The distribution of the angular velocity of Iaffaldano and DeMets (2016) is shown in red.

The effect of the viscosity models on the angular velocity outcomes of the California model is the similar to the case of the Pacific plate. Again, viscosity model 3 produces the largest angular velocity and viscosity model 1 the lowest. These models include an asthenosphere with the largest and lowest thickness.

8 Analysis of Results California hypothesis

As Figure 13 shows, the strength of the California plate boundary is doubled depending on which friction coefficient is used at 8 Ma. In any case the strength at 8 Ma is much larger than at 5 Ma. This is consistent with the developing boundary. The results of the torques at 8 and 5 Ma along the California boundary have been presented. The magnitude of the torques is what is expected for tectonic torques. What is opposite from the Pacific model is that the calculated torque at 8 Ma is larger than the torque at 5 Ma. The reason for this is that at 8 Ma the boundary conditions have been imposed in order to simulate the diffuse plate boundary present at that time. The large coefficient of friction leads to a large strength integral. The total torque is the sum of the torques along the plate boundary. So even though the modelled plate boundary is considerably smaller than in the Pacific model, the magnitude of the strength integral causes the total torque to be large.

The Euler vectors which describe the modelled North American motion change have been shown in Figure 15. The Euler poles overlap with the sampled poles from Iaffaldano and DeMets (2016). Therefore these outcomes are in favor of the hypothesis of the California boundary transformation as a cause of the North American motion change. The fit is not ideal, as the 68 percent confidence region of the model outcome lies on the outer edge of the results from the literature. Also the 20 percent confidence intervals are far apart. The angular velocity of the North American plate motion change correspond well with the result of Iaffaldano and DeMets (2016). The effect of the different friction coefficient and viscosity input models is similar as with the Pacific model. The calculated direction and magnitude of the Euler vectors of the model in general correspond well with the observed motion change of North America. It is a likely scenario that the absolute North American plate motion change is caused by the transformation of a diffuse margin to a fully developed strike-slip plate boundary in California.

9 Discussion

9.1 Model setup

The model is built to represent the characteristics of the Pacific-North America plate boundary in an accurate way. The strength profile which is constructed along the plate boundary depends on many different parameters. As mentioned in the method section, assumptions had to be made for parameters such as the heat flow of continents and the coefficient of friction. These assumptions introduce a factor of uncertainty. For the friction coefficient in this study it was decided to use a relationship with sediment thickness at the plate margin (Iaffaldano, 2012). This resulted in several models with a plausible range of friction coefficient values. Unfortunately not enough constraints of the friction coefficient are available to distinguish between the outcomes of the different input models. Furthermore, the models do not provide an estimate for the friction coefficient at continental boundaries. A reasonable value is

chosen in this case. This has an especially large influence on the results of the California model as in that case the whole modelled plate contact exists of continental lithosphere. In the context of modelling the strength of plate boundaries, better constraints on the friction coefficient would reduce the overall uncertainty of the strength integral tremendously.

Another large factor of uncertainty of the strength profile comes from laboratory measurements of ductile deformation parameters. The measurements deviate quite a lot between different studies. This has a large effect on the integral of the strength profile. The model is run for different values provided in the literature and the average of the strength integral is taken. Therefore it accounts for this uncertainty in a reasonable way. In general, the model of the strength profile is set up well as it includes the varying factors along the margin. Most input values of parameters were constrained accurately. Where data was unavailable or insufficient, reasonable assumptions were used.

For both hypotheses the same finite rotations were applied to describe the relative motion between the Pacific and North American plate. The choice of these Euler vectors have an effect on the model results as this motion defines the direction of the torque. The finite rotation of the North American absolute motion has a coarse resolution and is therefore the same for both 8 and 5 Ma. This makes that the North American motion change is not imposed as a condition in the model. This is rather a point of strength than a disadvantage. The resisting force of the Pacific plate is isolated which ensures that the torque difference solely depends on the Pacific plate motion. The finite rotations of Wessel and Kroenke (2008) do resolve the motion change of the Pacific plate between 8 and 5 Ma and are therefore a good choice for the model in this study. In the next section the implications of the effect of the viscosity on the model outcomes are discussed.

9.2 Viscosity

For both the Pacific and California model the same viscosity values have been used as an input. As described in the method section, a relationship with the viscosity contrast is used to estimate the asthenosphere thickness (Paulson and Richards, 2009). The asthenosphere thickness is included in the matrix $\mathbf{C}$ in the term $\frac{\mu_a}{D}$. In the inverted matrix $\mathbf{C}^{-1}$ the denominator and numerator are switched. $\frac{D}{\mu_a}$ is the final term which is included in the multiplication with the torque difference to get to the Euler vector change. This term shows that the asthenosphere thickness has a larger effect on the model than the viscosity contrast, which also can be observed in the outcome of the Pacific and California models. The viscosity model with the thinnest asthenosphere produces the lowest angular velocity, while the use of the model with the thickest asthenosphere results in the highest angular velocity. The viscosity structure in the mantle is relatively poorly understood. The tests with different viscosity models demonstrate that small deviations of values have a substantial effect on the magnitude of the calculated angular velocity in this study. This should be taken into consideration when working with such a model. Tighter approximations of the viscosity structure would help to get a better estimation of the angular velocity change caused by a change of torque.

9.3 The cause of the North American plate motion change

Two different hypotheses were proposed as a possible explanation of the North American plate motion change. In the first hypothesis it was suggested that the rotation of the Pacific plate has led to the motion change. The motion change of North America caused by the torque redistribution at the plate contact due to this event was calculated. As it turned out, the model results did not match the observed absolute motion change of the North American plate. The locations of the modelled Euler poles were far off from what was estimated by Iaffaldano and DeMets (2016).

The second hypothesis was based on the transformation of the plate contact in California. The direction of the North American motion change as a result of the tectonic evolution in California corresponded much better with the estimates in the literature. Although the fit was not perfect, the Euler vectors from the model matched the estimated Euler vectors well and therefore this could be a plausible explanation for the motion change of North America. The coefficient of friction plays an important role in the model as it is used to simulate the boundary in California at 8 Ma. An accurate estimate of the friction coefficient of such a boundary is unavailable and it was chosen to test the model for a range of values. Although the choice of this input value has an effect on the angular velocity, the direction of the motion does not change considerably. This means that even though the boundary characteristics are difficult to constrain, the model results still correspond well with the results of Iaffaldano and DeMets (2016). Therefore the boundary transformation in California seems to be a good explanation for the observed absolute motion change of the North American plate.

9.4 Rapid plate motion changes: an insight in torques affecting plates

Every motion change of a tectonic plate is caused by a change of torque working on that plate. In this study it has been demonstrated how rapid plate motion changes can be used to describe the responsible torque change. When motion changes occur within a relatively short time span (on a geological time scale), we can assume that some torques

affecting the plate have remained unchanged. This is useful because then only a physical description of the changing torques is required. A more accurate description the torque change leads to a more accurate approximation of the motion change induced by the torque difference. The approach of Iaffaldano and Bunge (2015) has shown to be a flexible method as it can be applied to many situations where different plate boundary processes play a role. This study also addressed some current limitations which should be taken into account while working with these models. With the rise of high-resolution plate reconstructions, the method applied in this study is a powerful tool and can be applied in the future to more tectonic scenarios.

10 Conclusion

With the use of a numerical model of the Pacific-North American plate boundary different scenarios have been tested which could explain the absolute motion change of North America in the Late Neogene. The torque exerted by the Pacific plate on the North American plate was reconstructed for 8 and 5 Ma. This involved the relative motion between the plates and the strength of the Pacific lithosphere at the boundary with North America. Based on the difference between these torques the Euler vector change of the North American plate has been calculated. The model outcomes do not overlap the motion change observed by Iaffaldano and DeMets (2016). Therefore it can be concluded that the rotation of the Pacific plate did not cause the absolute motion change of North America between 8 and 5 Ma. In a second scenario, the transformation of the plate contact in California was tested as a possible cause for the North American motion change. The model outcomes correspond well with the findings of Iaffaldano and DeMets (2016) which suggests that this is a plausible explanation for the North American motion change. The parameters in the model which result in the most uncertainty of the outcomes are the coefficient of friction of the plate boundary and the viscosity of the mantle.

11 Acknowledgements

First I would like to thank Giampiero Iaffaldano for the warm welcome and collaboration at the University of Copenhagen. This project would have been possible without his guidance. Furthermore, I would like to thank Rob Govers for the possibility of this thesis and his critical comments. At last, I would like to thank Juan Martín de Blas, Ingo Stotz and Valentina Espinoza Fernandez for many hours of good discussion with cake and coffee.

References

Austermann, J., Ben-Avraham, Z., Bird, P., Heidbach, O., Schubert, G., and Stock, J. M. (2011). Quantifying the forces needed for the rapid change of pacific plate motion at 6 ma. *Earth and Planetary Science Letters*, 307(3-4):289–297.

Bevis, M., Taylor, F. W., Schutz, B., Recy, J., Isacks, B., Helu, S., Singh, R., Kendrick, E., Stowell, J., Taylor, B., et al. (1995). Geodetic observations of very rapid convergence and back-arc extension at the tonga arc. *Nature*, 374(6519):249.

Bird, P. (2003). An updated digital model of plate boundaries. *Geochemistry, Geophysics, Geosystems*, 4(3).

Bunge, H.-P., Richards, M. A., Lithgow-Bertelloni, C., Baumgardner, J. R., Grand, S. P., and Romanowicz, B. A. (1998). Time scales and heterogeneous structure in geodynamic earth models. *Science*, 280(5360):91–95.

Burov, E. B. (2011). Rheology and strength of the lithosphere. *Marine and Petroleum Geology*, 28(8):1402–1443.

Byerlee, J. (1978). Friction of rocks. In *Rock friction and earthquake prediction*, pages 615–626. Springer.

Cande, S. C., Raymond, C. A., Stock, J., and Haxby, W. F. (1995). Geophysics of the pitman fracture zone and pacific-antarctic plate motions during the cenozoic. *Science*, 270(5238):947–953.

Cathles, L. M. (1975). *Viscosity of the Earth's Mantle*, volume 1362. Princeton University Press.

Chopra, P., Paterson, and MS (1981). The experimental deformation of dunite. *Tectonophysics*, 78(1-4):453–473.

Chopra, P. and Paterson, M. (1984). The role of water in the deformation of dunite. *Journal of Geophysical Research: Solid Earth*, 89(B9):7861–7876.

Christensen, N. I. and Mooney, W. D. (1995). Seismic velocity structure and composition of the continental crust: A global view. *Journal of Geophysical Research: Solid Earth*, 100(B6):9761–9788.

Cox, A. and Engebretson, D. (1985). Change in motion of pacific plate at 5 myr bp. *Nature*, 313(6002):472.

Croon, M. B., Cande, S. C., and Stock, J. M. (2008). Revised pacific-antarctic plate motions and geophysics of the menard fracture zone. *Geochemistry, Geophysics, Geosystems*, 9(7).

Davies, J. H. (2013). Global map of solid earth surface heat flow. *Geochemistry, Geophysics, Geosystems*, 14(10):4608–4622.

DeMets, C., Iaffaldano, G., and Merkouriev, S. (2015a). High-resolution neogene and quaternary estimates of nubia-eurasia-north america plate motion. *Geophysical Journal International*, 203(1):416–427.

DeMets, C. and Merkouriev, S. (2016). High-resolution reconstructions of pacific–north america plate motion: 20 ma to present. *Geophysical Journal International*, 207(2):741–773.

DeMets, C., Merkouriev, S., and Sauter, D. (2015b). High-resolution estimates of southwest indian ridge plate motions, 20 ma to present. *Geophysical Journal International*, 203(3):1495–1527.

Doubrovine, P. V., Steinberger, B., and Torsvik, T. H. (2012). Absolute plate motions in a reference frame defined by moving hot spots in the pacific, atlantic, and indian oceans. *Journal of Geophysical Research: Solid Earth*, 117(B9).

Fletcher, J. M., Grove, M., Kimbrough, D., Lovera, O., and Gehrels, G. E. (2007). Ridge-trench interactions and the neogene tectonic evolution of the magdalena shelf and southern gulf of california: Insights from detrital zircon u-pb ages from the magdalena fan and adjacent areas. *Geological Society of America Bulletin*, 119(11-12):1313–1336.

Gleason, G. C. and Tullis, J. (1995). A flow law for dislocation creep of quartz aggregates determined with the molten salt cell. *Tectonophysics*, 247(1-4):1–23.

Hager, B. and Richards, M. (1989). Long-wavelength variations in earth's geoid: physical models and dynamical implications. *Philosophical Transactions of the Royal Society of London. Series A, Mathematical and Physical Sciences*, 328(1599):309–327.

Hirth, G. and Kohlstedt, D. L. (1996). Water in the oceanic upper mantle: implications for rheology, melt extraction and the evolution of the lithosphere. *Earth and Planetary Science Letters*, 144(1-2):93–108.

Iaffaldano, G. (2012). The strength of large-scale plate boundaries: Constraints from the dynamics of the philippine sea plate since 5 ma. *Earth and Planetary Science Letters*, 357:21–30.

Iaffaldano, G. and Bunge, H.-P. (2015). Rapid plate motion variations through geological time: Observations serving geodynamic interpretation. *Annual Review of Earth and Planetary Sciences*, 43:571–592.

Iaffaldano, G. and DeMets, C. (2016). Late neogene changes in north america and antarctica absolute plate motions inferred from the mid-atlantic and southwest indian ridges spreading histories. *Geophysical Research Letters*, 43(16):8466–8472.

Iaffaldano, G., Hawkins, R., Bodin, T., and Sambridge, M. (2014). Redback: Open-source software for efficient noise-reduction in plate kinematic reconstructions. *Geochemistry, Geophysics, Geosystems*, 15(4):1663–1670.

Kirby, S. H. (1983). Rheology of the lithosphere. *Reviews of Geophysics*, 21(6):1458–1487.

Kohlstedt, D., Evans, B., and Mackwell, S. (1995). Strength of the lithosphere: Constraints imposed by laboratory experiments. *Journal of Geophysical Research: Solid Earth*, 100(B9):17587–17602.

Koppers, A. A., Staudigel, H., Wijbrans, J. R., and Pringle, M. S. (1998). The magellan seamount trail: implications for cretaceous hotspot volcanism and absolute pacific plate motion. *Earth and Planetary Science Letters*, 163(1-4):53–68.

Lu, L. X. and Jiang, D. (2019). Quartz flow law revisited: The significance of pressure dependence of the activation enthalpy. *Journal of Geophysical Research: Solid Earth*, 124(1):241–256.

Luan, F. and Paterson, M. (1992). Preparation and deformation of synthetic aggregates of quartz. *Journal of Geophysical Research: Solid Earth*, 97(B1):301–320.

McKenzie, D., Jackson, J., and Priestley, K. (2005). Thermal structure of oceanic and continental lithosphere. *Earth and Planetary Science Letters*, 233(3-4):337–349.

Michaud, F., Royer, J.-Y., Bourgois, J., Dyment, J., Calmus, T., Bandy, W., Sosson, M., Mortera-Gutiérrez, C., Sichler, B., Rebolledo-Viera, M., et al. (2006). Oceanic-ridge subduction vs. slab break off: Plate tectonic evolution along the baja california sur continental margin since 15 ma. *Geology*, 34(1):13–16.

Mitrovica, J. X. (1996). Haskell [1935] revisited. *Journal of Geophysical Research: Solid Earth*, 101(B1):555–569.

Müller, R. D., Sdrolias, M., Gaina, C., Steinberger, B., and Heine, C. (2008). Long-term sea-level fluctuations driven by ocean basin dynamics. *science*, 319(5868):1357–1362.

Oskin, M. and Stock, J. (2003a). Marine incursion synchronous with plate-boundary localization in the gulf of california. *Geology*, 31(1):23–26.

Oskin, M. and Stock, J. (2003b). Pacific–north america plate motion and opening of the upper delfín basin, northern gulf of california, mexico. *Geological Society of America Bulletin*, 115(10):1173–1190.

Oskin, M., Stock, J., and Martín-Barajas, A. (2001). Rapid localization of pacific–north america plate motion in the gulf of california. *Geology*, 29(5):459–462.

Paulson, A. and Richards, M. A. (2009). On the resolution of radial viscosity structure in modelling long-wavelength postglacial rebound data. *Geophysical Journal International*, 179(3):1516–1526.

Peltier, W. and Jiang, X. (1996). Mantle viscosity from the simultaneous inversion of multiple data sets pertaining to postglacial rebound. *Geophysical Research Letters*, 23(5):503–506.

Pollack, H. N., Hurter, S. J., and Johnson, J. R. (1993). Heat flow from the earth's interior: analysis of the global data set. *Reviews of Geophysics*, 31(3):267–280.

Richards, M. A. and Lenardic, A. (2018). The cathles parameter (ct): A geodynamic definition of the asthenosphere and implications for the nature of plate tectonics. *Geochemistry, Geophysics, Geosystems*, 19(12):4858–4875.

Robertson, E. C. (1988). Thermal properties of rocks.

Rutter, E. and Brodie, K. (2004). Experimental intracrystalline plastic flow in hot-pressed synthetic quartzite prepared from brazilian quartz crystals. *Journal of Structural Geology*, 26(2):259–270.

Stein, C. A. and Stein, S. (1992). A model for the global variation in oceanic depth and heat flow with lithospheric age. *Nature*, 359(6391):123.

Stock, J. and Hodges, K. (1989). Pre-pliocene extension around the gulf of california and the transfer of baja california to the pacific plate. *Tectonics*, 8(1):99–115.

Stotz, I. L., Iaffaldano, G., and Davies, D. (2017). Late miocene pacific plate kinematic change explained with coupled global models of mantle and lithosphere dynamics. *Geophysical Research Letters*, 44(14):7177–7186.

Suppe, J. (2007). Absolute fault and crustal strength from wedge tapers. *Geology*, 35(12):1127–1130.

Torsvik, T. H., Steinberger, B., Gurnis, M., and Gaina, C. (2010). Plate tectonics and net lithosphere rotation over the past 150 my. *Earth and Planetary Science Letters*, 291(1-4):106–112.

Umhoefer, P. J. (2011). Why did the southern gulf of california rupture so rapidly?—oblique divergence across hot, weak lithosphere along a tectonically active margin. *GSA today*, 21(11):4–10.

Van Wijk, J., Axen, G., and Abera, R. (2017). Initiation, evolution and extinction of pull-apart basins: Implications for opening of the gulf of california. *Tectonophysics*, 719:37–50.

Wessel, P. and Kroenke, L. W. (2008). Pacific absolute plate motion since 145 ma: An assessment of the fixed hot spot hypothesis. *Journal of Geophysical Research: Solid Earth*, 113(B6).

White, R. S., McKenzie, D., and O'Nions, R. K. (1992). Oceanic crustal thickness from seismic measurements and rare earth element inversions. *Journal of Geophysical Research: Solid Earth*, 97(B13):19683–19715.

Whittaker, J. M., Goncharov, A., Williams, S. E., Müller, R. D., and Leitchenkov, G. (2013). Global sediment thickness data set updated for the australian-antarctic southern ocean. *Geochemistry, Geophysics, Geosystems*, 14(8):3297–3305.

Wilks, K. R. and Carter, N. L. (1990). Rheology of some continental lower crustal rocks. *Tectonophysics*, 182(1-2):57–77.

Appendices

A - Ductile deformation parameters

The explanation and units of the different ductile parameters used in this study can be found in Table 4. For the gas constant the value 8.314 $J \cdot K^{-1} \cdot mol^{-1}$ is used. The parameter V_d is kept constant at $17 \cdot 10^{-6} m^3/mol$. The values of the other parameters are shown in Table 5.

Parameter	Description	Unit
n	Constant characteristic of the creep process	$-$
A	Material parameter	$MPa^{-n}s^{-1}$
Q	Activation energy	J/mol
V_d	Activation volume	m^3/mol
R	Gas constant	$J \cdot K^{-1} \cdot mol^{-1}$

Table 4: Description and units of the different parameters affecting the plastic strength in the model.

Rock type	**n (-)**	**A** $(MPa^{-n}s^{-1})$	**Q (kJ/mol)**	**Source**
Wet Quartzite	4.0	$1.1 \cdot 10^{-4}$	223	Gleason and Tullis (1995)
	2.97	$3.55 \cdot 10^{-3}$	242	Rutter and Brodie (2004)
	4	$1.19 \cdot 10^{-8}$	152	Luan and Paterson (1992)
	4	$6 \cdot 10^{-11}$	132	Lu and Jiang (2019)
Wet Olivine	4.45	275.6	498	Chopra and Paterson (1984)
	3.5	$4.88 \cdot 10^{6}$	515	Hirth and Kohlstedt (1996)
	4.5	2.6	498	Evans & Kohlstedt (1995)
Gabbro	3.4	$5 \cdot 10^{9}$	497	Wilks and Carter (1990)
	3.4	$10^{-3.7}$	260	Kirby (1983)
	3.4	$2 \cdot 10^{-4}$	260	Kirby (1983)

Table 5: The ductile parameter values used as input in the model.

B - Derivation of the torque balance

As mentioned in the Method section, the net torque $\mathbf{M}_T$ is the sum of the torques caused by shallow-seated (tectonic) forces ($\mathbf{M}_N$) and the torques caused by basal-shear (asthenosphere) forces ($\mathbf{M}_b$).

$$\mathbf{M}_T = \mathbf{M}_N + \mathbf{M}_b$$

The total torque can be linked to the moment of inertia through Newton's second law of motion. This law describes how much an object will accelerate when a certain force is applied. In this context, the moment of inertia of a plate is a measure for the resistance of the rotation around an axis. This leads to the following equation:

$$\mathbf{M}_T = \mathbf{I}_p \cdot \frac{d\boldsymbol{\omega}(t)}{dt} \tag{18}$$

Where $\mathbf{I}_p$ is the plate moment of inertia and the vector $\boldsymbol{w}(t)$ represents the angular velocity. In most cases it is impossible to solve Equation 18 directly. We do can get a sense of the magnitude of the value for $\mathbf{M}_T$ at a certain moment in time. Equation 18 can be rewritten to a first order ordinary differential equation.
An elaboration on this process can be found in the Supplementary Information of Iaffaldano and Bunge (2015). The solution takes the form $\omega(t) = \omega_e \cdot (1 - e^{-\frac{t}{\tau}})$, where τ is the characteristic equilibrium time of the solution. An upper limit for τ is defined as:

$$\tau = \frac{5R_e^2 \rho_M h_M D_M}{\mu_m (R_e - h_M)^2} \tag{19}$$

Where R_e is the radius of the Earth and D_M the maximum depth of the asthenosphere. ρ_M and h_M are the maximum density and thickness of the tectonic plate. Finally, μ_m is the minimum viscosity of the asthenosphere. When Earth-like

values for these values are chosen, a maximum value for τ can be estimated with reasonable certainty. As it turns out, $\tau < 10^{-1}$ seconds. This means that on a geological timescale, the time it takes for plates to adjust to torque changes is negligible. In other words, at every moment in time a torque balance exists:

$$\mathbf{M}_N + \mathbf{M}_b = 0 \tag{20}$$

C - Sensitivity Euler vectors for friction coefficient and viscosity

The angular velocity and Euler poles are shown in the histograms. The angular velocity plots are described previously in the study. The location of the Euler poles is barely affected by the coefficient of friction models. The longitudes and latitudes do not change at all for different viscosity models. The results of the Pacific model are shown in Figure 18. The results of the California model are shown in Figure 19.

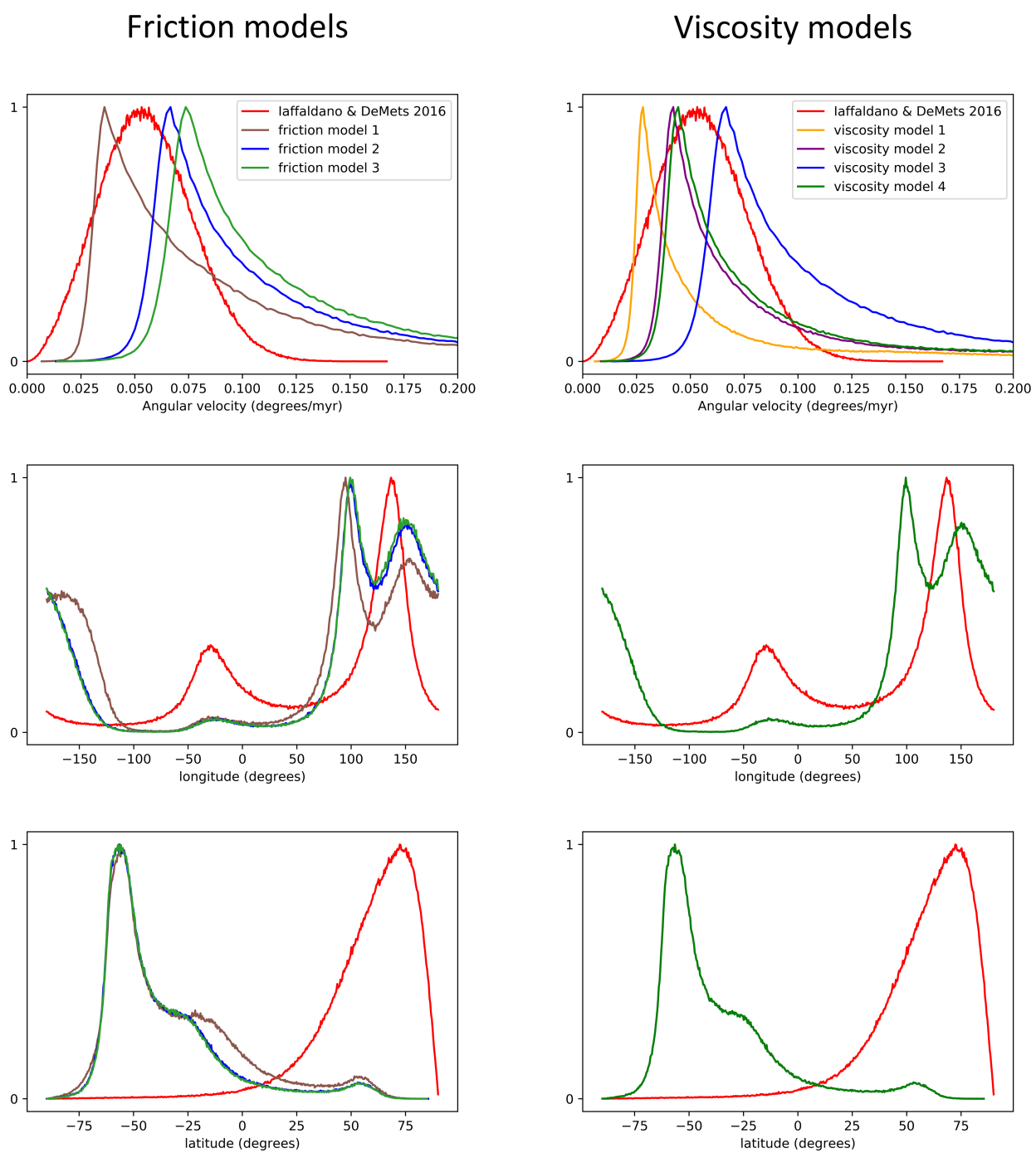

Figure 18: The effect of the friction models (left) and viscosity models (right) on the outcomes of the Pacific model. The histograms show the angular velocity and longitude and latitude of the Euler poles. Different colours correspond with different models. The results of Iaffaldano and DeMets (2016) are shown in red.

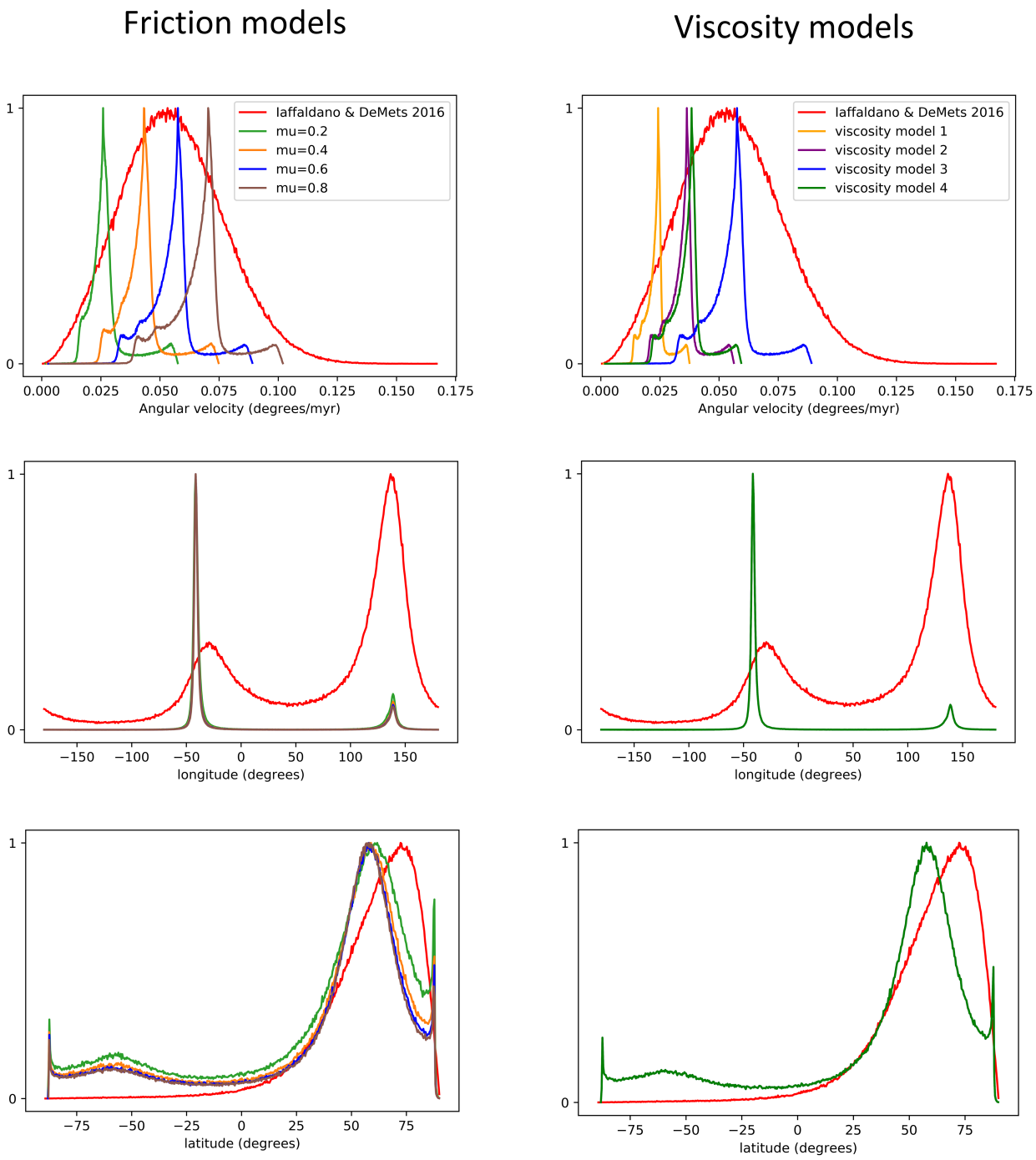

Figure 19: The effect of the friction models (left) and viscosity models (right) on the outcomes of the California model. The histograms show the angular velocity and longitude and latitude of the Euler poles. Different colours correspond with different models. The results of Iaffaldano and DeMets (2016) are shown in red.